Study of a Night Sky Radiator Cooling System Utilizing Direct Fluid Radiation Emission and Varying Cover Materials

By

William Overmann

A Thesis Presented in Partial Fulfillment
of the Requirements for the Degree
Master of Science

Approved November 2011 by the
Graduate Supervisory Committee:

Patrick Phelan, Chair
Robert Taylor
Steven Trimble

ARIZONA STATE UNIVERSITY

December 2011

ABSTRACT

As the demand for power increases in populated areas, so will the demand for water. Current power plant technology relies heavily on the Rankine cycle in coal, nuclear and solar thermal power systems which ultimately use condensers to cool the steam in the system. In dry climates, the amount of water to cool off the condenser can be extremely large. Current wet cooling technologies such as cooling towers lose water from evaporation. One alternative to prevent this would be to implement a radiative cooling system. More specifically, a system that utilizes the volumetric radiation emission from water to the night sky could be implemented. This thesis analyzes the validity of a radiative cooling system that uses direct radiant emission to cool water. A brief study on potential infrared transparent cover materials such as polyethylene (PE) and polyvinyl carbonate (PVC) was performed. Also, two different experiments to determine the cooling power from radiation were developed and run. The results showed a minimum cooling power of 33.7 W/m^2 for a vacuum insulated glass system and 37.57 W/m^2 for a tray system with a maximum of 98.61 Wm^{-2} at a point when conduction and convection heat fluxes were considered to be zero. The results also showed that PE proved to be the best cover material. The minimum numerical results compared well with other studies performed in the field using similar techniques and materials. The results show that a radiative cooling system for a power plant could be feasible given that the cover material selection is narrowed down, an ample amount of land is available and an economic analysis is performed proving it to be cost competitive with conventional systems.

Thanks to my friends and family for putting up with me.

ACKNOWLEDGMENTS

Dr. Patrick Phelan provided much input and support throughout the process of this thesis. Many of my fellow lab colleagues provided valuable insight and a helping hand including Rob, Jon, Andrey, Mark W, Mark M, Brent, Carlos, Erin, Wei and Aziz, as well as others. Thank you to all involved.

TABLE OF CONTENTS

Page

LIST OF TABLES

Table Page

LIST OF FIGURES

Figure Page

Figure Page

NOMENCLATURE

A	area	[m^2]
c_o	speed of light in a vacuum	[m/s]
c_p	specific heat at constant pressure	[J/kg/K]
E	emissive power	[W/m^2]
$\dot{E}$	rate of thermal and mechanical energy transfer	[W]
h	convective heat transfer coefficient	[$W/m^2/K$]
h	universal Planck constant	[J·s]
I	radiation intensity	[$W/m^2/sr$]
k	Boltzmann constant	[J/K]
q	heat transfer rate	[W]
$q"$	heat flux	[W/m^2]
$R\downarrow$	atmospheric downwelling thermal radiation	[W/m^2]
T	temperature	[^oC]
t	time	[s]
V	volume	[m^3]
x, y, z	rectangular coordinates	[m]

Greek Symbols

η	wavenumber	[cm^{-1}]
ρ	density	[kg/m^3]
λ	wavelength	[μm]
ε	emissivity	dimensionless
σ	Stefan-Boltzmann constant	[$W/m^2/K^4$]

Subscripts

b	blackbody
dp	dew point
db	dry bulb
rad	radiation

st	stored
sur	surroundings

INTRODUCTION

Motivation

Radiative cooling has been occurring from the beginning of time. Objects and areas give off heat in the form of radiation because of simple laws of nature. The desert is a prime example of radiative cooling and how effective it can be. Deserts in the southwest United States can reach temperatures over 43 degrees Celsius during the day, while at night the temperature can reach around 16 degrees Celsius lower.

Current radiative cooling techniques involve not only radiation, but conduction and convection as well. Typically, the fluid in the system is either water or air. In systems with air as the fluid, a radiator is placed on top of the area being cooled. The warm air rises and is transferred through convection to a metal radiator typically made of aluminum. (Michell & Biggs, 1979) The heat then conducts to the other side of the metal and is radiated to the night sky. This type of setup can be seen in *Figure 1*. It should be noted that the term *night sky* relates to the effective sky temperature, T_{sky}, which is based upon conditions in the atmosphere such as cloudiness and moisture content. The temperature can reach as low as 230 K. (Incropera, Dewitt, Bergman, & Lavine, 2007) An expression for T_{sky} will be discussed later in the paper.

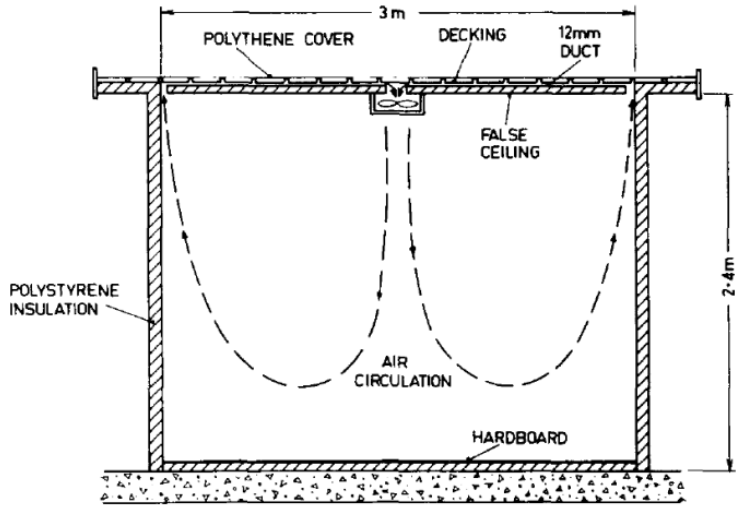

Figure 1. Setup of air cooling radiator room (Michell & Biggs, 1979)

All radiators have a working fluid and often times that fluid is water. Typically piping is used to remove heat from a specified area by transferring heat to the water and then the water flows to the radiating portion of the system. Again, the radiator is typically aluminum and the heat is transferred to allow for the aluminum to radiate heat to the sky as shown in *Figure 2*.

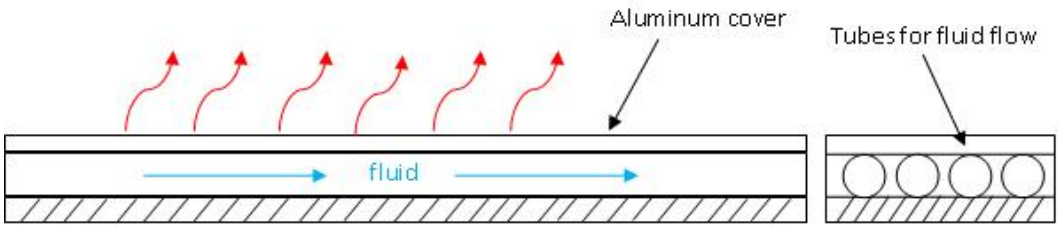

Figure 2. Diagram of conventional aluminum radiator cooling system

The aluminum can be covered in a material such as black paint to create more of a black body effect during radiation, resulting in higher emission. (Kimball, 1985) To reduce heat gain from convection, cover materials are placed over the top of the radiator and the sides are built higher to create an air gap between the radiator and cover. Materials such as polycarbonate and polyethylene are used because they can be fairly cheap and have a high transmittance in the ideal wavelength range. (Ali, Taha, & Ismail, 1995) The ideal wavelength range will be discussed further in the sections covering atmospheric radiation and Planck's Law.

Objective

Current radiative cooling techniques involve a minimum of three modes of heat transfer. From the example above, the three heat transfer modes are convection from air to metal, conduction through the metal, and finally radiation to the sky. Implementing a system that directly radiates heat from the fluid removes conduction through metal from the process as well as the metal from the system. A system with a material that has high transmittance in the proper infrared (IR) range, such as polyethylene (PE) or polyvinyl chloride (PVC), can allow the water to directly radiate heat to the night sky. This would decrease the cost of a large radiator system and potentially make the system more efficient due to avoiding an extra mode of heat transfer. The objective is to design and build experiments that determine the cooling power of a direct fluid

radiative system. Comparisons are then made to current radiant cooling technologies and the practicality of the system is determined.

Potential for Utilities

Engineers can utilize this radiative cooling technique to cool homes, warehouses, factories, office buildings, and even power plants. More specifically to power plants, radiation can be a useful method for cooling condensers. The water needed to cool a condenser typically has a change in temperature of 10 ^{o}C, which is not an extremely high value for a radiative system to achieve. (Culp, 1991) The majority of current cooling technology utilizes water and consists of cooling towers as well as capturing flowing water from rivers and streams for cooling. There are also plants that use dry cooling (convection with air) and it should be noted that they are not as efficient as wet cooling systems and ultimately lead to lower overall plant efficiencies. (El-Wakil, 2002)

The prominent methods of cooling condensers using water are single-pass cooling from rivers and streams, single-pass cooling from artificial ponds, and cooling towers. (Culp, 1991) These methods have their own drawbacks. Single pass cooling from rivers and streams, while very efficient, causes thermal pollution that can negatively affect the wildlife in the flowing rivers and streams. Cooling towers and artificial cooling ponds are effective based on the principal of evaporation which consequently means there needs to be some amount of make-up water each time the water cycles through. Evaporation can result in a 1% to 1.5% loss of water for every cycle. (El-Wakil, 2002) This may not seem like a significant amount, but an example with quantitative values may make this more eye opening. Consider a 1000 MW power plant that utilizes wet cooling towers. These cooling towers circulate roughly 49,520 Ls^{-1} of water. In a hot climate such as the Southwestern United States, evaporation losses turn out to be around 631 Ls^{-1} of water. (El-Wakil, 2002) If this power plant is running at full power for 12 hours, the loss of water due to evaporation is 27.26 million liters. And there will be more water lost from evaporation during the other 12 hours the plant runs, although not at full power.

One potential solution for power plant cooling issues in areas where water is a precious resource is a radiative cooling system. Instead of using dry or wet cooling towers, a field of

radiators could be used to dissipate the heat to the sky at nighttime, and with further research, potentially even during the daytime.

Background

There have been many publications on radiative cooling. Unfortunately, there has not been a break through formula or method for radiative cooling that has caught on and made it to the marketplace. However, there are many promising ideas in the field and they are discussed below.

Cooling buildings via radiative transfer is a concept that has been studied for years. One study conducted an experiment that compared two huts identical in structure, but with different roof coverings. (Michell & Biggs, 1979) One hut was built with a steel roof that was painted with a specific white coating to act as a selective surface coating which reflected certain wavelengths and emitted other wavelengths. The other hut roof was made of aluminum and given a special coating to make it absorb and emit within the appropriate atmospheric window of 8 to 13 μm. (For a better understanding of the atmospheric window, see the section Atmospheric Radiation.) The experiment was run at night and the results showed that the roofs yielded similar cooling performance and achieved 22 Wm^{-2} overall in radiative cooling power. The actual cooling was higher, but convection losses contributed to the decrease in cooling power. More importantly, this publication found that there was little difference between a blackbody radiator and a selective surface radiator.

Another method of cooling buildings utilizes a small pond on the rooftop to collect the heat that has risen inside the building. (Erell & Etzion, 2000) The heat can then be directly radiated from the pond or it can be run through a system of fabricated radiators. An experiment with this method used three commercially available solar collectors with some modifications to perform as radiators. Water from a roof pond was circulated through the collectors during the nighttime and inlet and outlet temperatures were recorded. The experiment did not explicitly show temperature loss from radiation, but it can be inferred from data that showed a 1.5 ^{o}C increase in ambient temperature while the fluid temperature only rose between 0.05 ^{o}C to 0.4 ^{o}C over the same period of time. While this publication did not provide astonishing results, it did reveal that

coupling night time radiators with daytime solar collectors is within the realm of possibility and should be studied further.

One of the more interesting concepts of radiative cooling is the application of a radiator for cooling to the sky during the daytime. The issue with this concept is that trying to keep incoming radiation from heating up the radiator is extremely difficult. Proper selective surface materials are needed so that an atmospheric window will only allow certain wavelengths to transfer. This is realized theoretically through Planck's Law which will be discussed later. One publication detailed an experiment that utilized a radiative cooling system for air for 24 hours in a location near the equator. (Nilsson & Niklasson, 1995) The radiators were insulated boxes with heaters built in and utilized various covers that were shown to have high reflectance to solar wavelengths and high transmittance in the infrared range. All covers were varied in thickness. The results showed that a cover containing zinc sulfide (ZnS), which happened to be the thickest, was able to perform cooling over 19 hours of the day and allowed for the least amount of heating around the middle of the day at only 7.2 W/m^2. However, the thinner covers were able to make up for this by cooling more effectively during the nighttime hours. Even though the ZnS cover successfully cooled over 19 hour of the day, its modified selective surface properties mean that it would be very expensive to produce and therefore not currently feasible. Unfortunately the publication did not mention the exact price.

Other studies have been done to evaluate the effect of a flowing system for cooling water via radiation. One experiment that was run used a gravity-fed water flowing system. (Ali, Taha, & Ismail, 1995) The water was run through parallel plates with the top plate being the radiator made of aluminum and painted black. The radiator was covered with different types of polyethylene to prevent convective losses. The system with the thinner polyethylene cover had an average cooling power of 32.7 W/m^2 during the nighttime hours. The authors also concluded that flowing systems were more efficient than stagnant cooling systems for two reasons; higher convective resistance between plate and water when not flowing and the inlet water temperature is warmer relative to the plate than the stagnant water.

In a similar experiment, solar collectors were used to alternately work as radiators during the night. (Matsuta, Terada, & Ito, 1987) To make this work, the cover was made of a spectrally selective surface. The publication claimed a cooling radiation flux of 51 W/m^2 on a clear night, while still achieving 610 W/m^2 of solar collective flux in good conditions. This study gives promise to the concept of having a solar thermal collector during the day act as a sky radiator during the night, thus making use of all 24 hours in a day.

One final publication to mention also backs up the claims made by Matsuta *et al.* An experiment was performed testing a panel made for both daytime solar collecting and nighttime radiation cooling. (Yiping, Yong, Li, & Lijun, 2008) The novel part of this experiment was that the collector/radiator was designed as a structural element as well and can be integrated into the building as a support. More importantly, the experiment resulted in a cooling capacity of 50 W/m^2 with a polyethylene or polycarbonate cover and 47 W/m^2 without any cover. A summary of the results found from the publications mention can be seen in Table 1.

Table 1. *Summary of published sky radiator data*

Author(s)	**Year**	**Description**	**Result**
Michell & Biggs	1979	Two huts with different material radiators	**22 W/m^2**
Matsuta et al.	1987	Solar collectors/sky radiators	**51 W/m^2**
Ali et al.	1995	Gravity fed aluminum radiator	**32.7 W/m^2**
Yiping et al.	2008	Model of solar collector/sky radiator	**50 W/m^2**
Nilsson & Niklasson	1995	Box radiators with daytime cooling	**19 hours of cooling**

Methodology

A simple order was used for the structure of the experiments in this thesis and can be seen in the flow chart shown in *Figure 3*. Once the general topic of radiation was chosen, the concept of using direct fluid emission for cooling was selected as a specific area of study. The first step was to determine the materials to be used for the covers of the radiators. A simple experiment analyzing different materials with an infrared camera was performed. These materials were narrowed down to the ones that showed promise for being the most transparent in the infrared wavelengths of light. The selected materials, PVC and two different PEs, were analyzed with a Fourier Transform Infrared (FTIR) spectrometer and the top two materials, both PEs, were used

for the experiments. The first experiment run was on a small scale and involved vacuum insulated glass (VIG) cylinders filled with water. This experiment was run to determine if the concept of direct radiation emission from a fluid was feasible. Once the concept was validated, the two chosen polyethylene materials were used as covers in the tray experiments which most closely simulated a scaled sky radiator. Finally, the best cover material was compared to a conventional metal covered radiator using the same tray experimental setup.

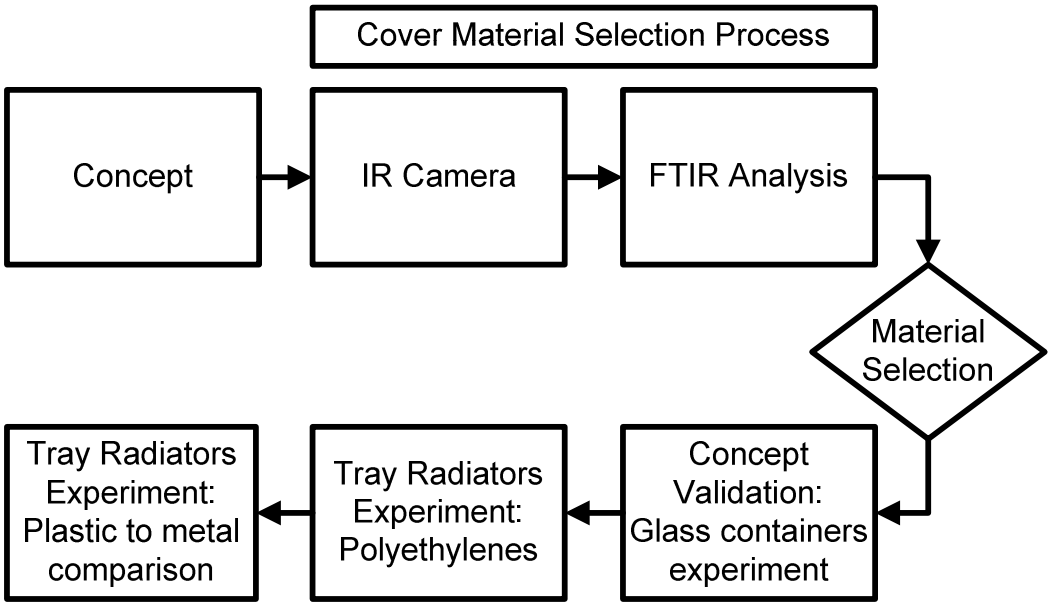

Figure 3. Flowchart for experimental process

Atmospheric Window

Due to certain physical properties of the atmosphere, radiating to the sky is possible. An atmospheric window exists between the wavelengths of 8 and 13 µm. This atmospheric window means that atmospheric radiation emission and absorption are very low compared to other wavelength ranges. Because these are so low, transmittance of thermal radiation can be very high. This can be seen in *Figure 4*. Wien's Displacement Law, which will be discussed further in the paper, shows that the peak radiation emission occurs around 10 µm because of the correlation where objects on Earth typically emit radiation between 250 and 320 K. (Mills, 1999) However, cloud cover can hamper the effect of radiation. Therefore, dry climates with minimal pollution would be ideal for the radiator cooling system proposed in this thesis.

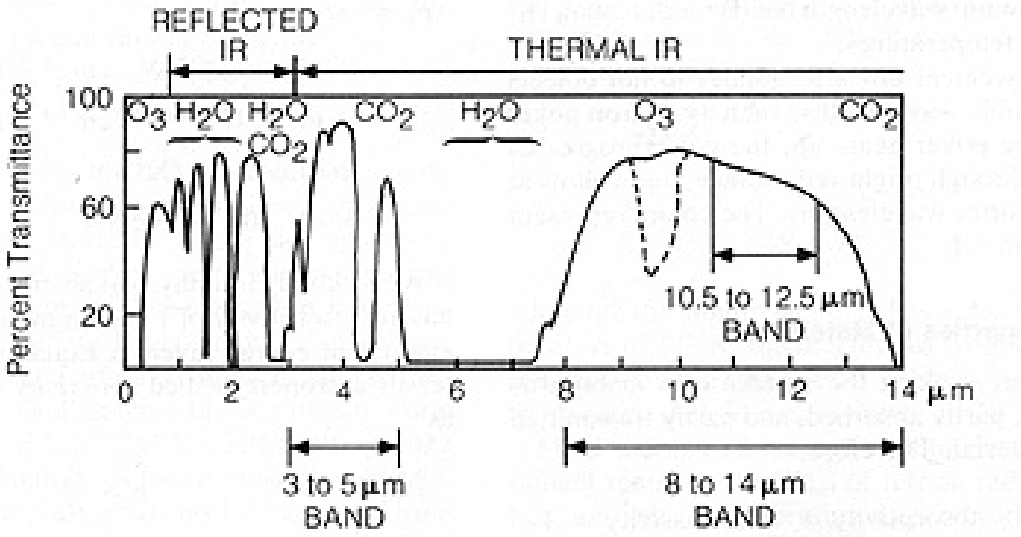

Figure 4. Percent transmittance of the Earth's Atmosphere (Short)

PLANCK'S LAW

Radiation plays a role in the heating and cooling of everything in the universe. Every object radiates over a spectrum of wavelengths, but will emit a maximum amount of radiation at a certain wavelength that is related to its current temperature. The relation between the wavelength and temperature is called Planck's Law. Planck's Law can be seen in Equation 1, (Incropera, Dewitt, Bergman, & Lavine, 2007)

$$I_{\lambda,b}(\lambda,T) = \frac{2hc_o^2}{\lambda^5\left[e^{\frac{hc_o}{\lambda kT}} - 1\right]} \quad (1)$$

where $I_{\lambda,\,b}$ is the blackbody spectral intensity, λ is the wavelength in a vacuum, T is the temperature, the universal Planck constant is $h = 6.626\text{x}10^{-34}$ J·s, the Boltzmann constant is $k = 1.318\text{x}10^{-23}$ JK^{-1}, and the speed of light in a vacuum is $c_o = 2.998\text{x}10^{8}$ ms^{-1}. Sometimes Planck's Law is written in terms of spectral blackbody emissive power, $E_{\lambda,\,b}$:

$$E_{\lambda,b}(\lambda,T) = \pi I_{\lambda,b}(\lambda,T) \quad (2)$$

A plot of $E_{\lambda,\,b}$ versus λ can be seen in *Figure 5*. Incropera et al. noted that the distribution has important characteristics. Those characteristics are the following:

> 1, the emitted radiation varies continuously with wavelength; 2, at any wavelength the magnitude of the emitted radiation increases with the increasing temperature; 3, the spectral region in which the radiation is concentrated depends on temperature, with comparatively more radiation appearing at shorter wavelengths as the temperature increases; 4, a significant fraction of the radiation emitted by the sun, which may be approximated as a blackbody at 5800 K, is in the visible region of the spectrum. In contrast, for T less than or about equal to 800 K, emission is predominantly in the infrared region of the spectrum and is not visible to the eye. (Incropera, Dewitt, Bergman, & Lavine, 2007, p. 737)

This last characteristic is very important to the work of this thesis.

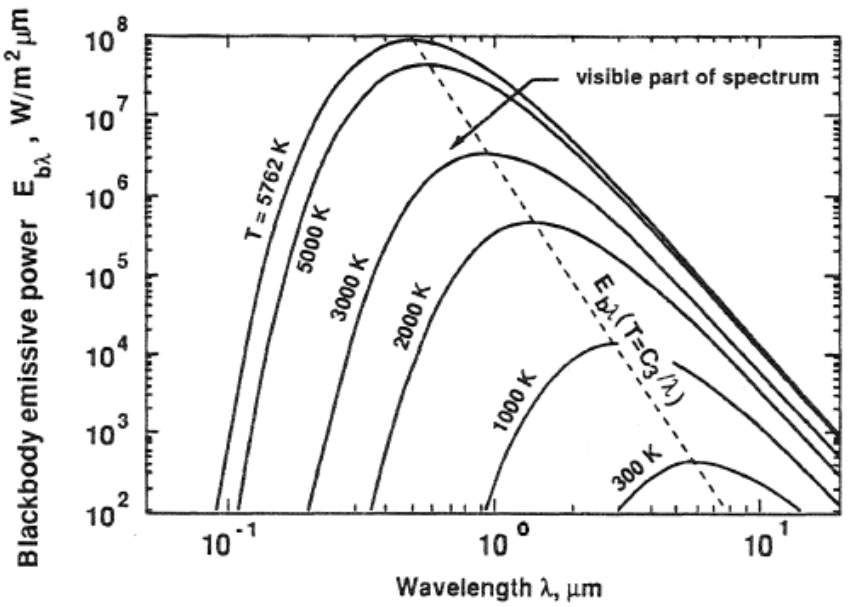

Figure 5. Blackbody emissive power over a broad light spectrum (Carvalho, 2010)

As stated earlier, the degree of temperature change from inlet to outlet of the cooling water will only be about 10 ^{o}C. Assuming that the water drawn up to enter the system is at ambient temperature, the range of temperatures can be estimated to be between 50 and 100 ^{o}F which converts to a range of 283 K to about 311 K. From these temperatures, the potential wavelengths that the water will radiate at were determined. To find these wavelengths, Wien's Displacement Law needs to be taken into account. The formula is

$$\lambda_{max} T = C_3 \tag{3}$$

where C_3 = 2898 μm·K and is called the third radiation constant. (Incropera, Dewitt, Bergman, & Lavine, 2007) For a temperature of 283 Kelvin, the maximum emissive power is at a wavelength of 10.2 μm. Water at a typical room temperature of 298 K has a maximum emissive power at 9.7 μm and if water were at 311 K, it would have a maximum emissive power at 9.3 μm. *Figure 6* shows the blackbody emissive power for a range of temperatures relevant to the radiant cooling system discussed in this thesis. The figure is the graphical interpretation of Planck's Law formulated by Matlab code. (Spetzler & Venables, 2004) It should be noted that the cover used in

the system must have a high transmittance in the wavelength range of 9 to 11 μm to have the highest possible emissive power transferred.

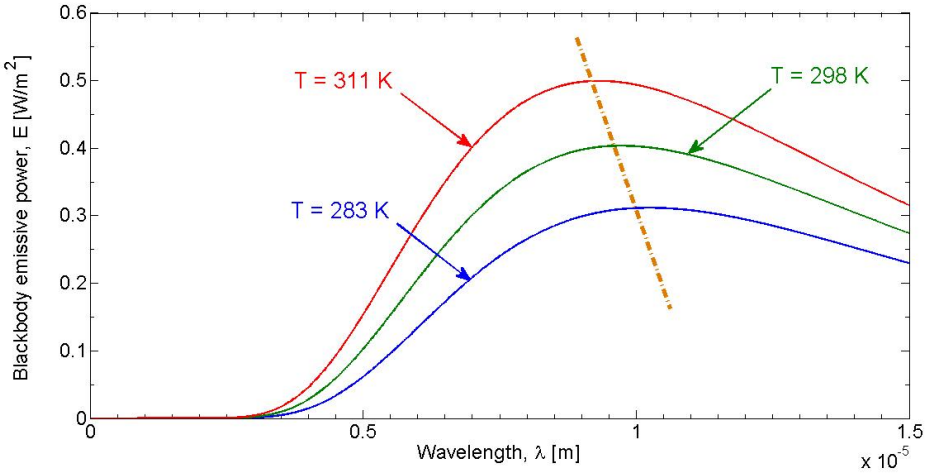

Figure 6. Blackbody emissive power at relevant cooling temperatures with the orange bar crossing at the maximum values of *E*

EFFECTIVE NIGHT SKY

An approximate net rate heat transfer equation for radiation can be given as (Incropera, Dewitt, Bergman, & Lavine, 2007)

$$q_{rad} = \sigma \varepsilon A(T_{source}^4 - T_{sur}^4) \quad (4)$$

where q_{rad} is the radiation heat transfer from the surface in W, σ = 5.670x10^{-8} Wm^{-2}K^{-1} is the Stefan-Boltzmann constant, ε is the emissivity of the source, A is the area of the emitting source in m^2, T_{source} is the temperature of the source in K, and T_{sur} is the temperature of the surroundings in K. Analyzing this equation, it becomes clear that there are many ways to increase q_{rad}. A larger surface area for radiating or a higher emissivity can increase the heat transfer rate. The other way to increase q_{rad} is to achieve a large difference between the temperature of the source of radiation and the temperature of the surroundings that are receiving the radiation (ΔT). Buildings and objects are typically at ambient temperature or may even be above if they have stored some heat due to being a large thermal mass and are not good for creating large ΔTs. To cool below ambient, a large heat sink is necessary. That heat sink is the night sky.

The equivalent night sky temperature, or effective night sky temperature, is somewhat unclear in the scientific community and has various models that try to predict it. Perez-Garcia provides the following for a definition:

> A simple model for the description of the general radiation budget between the atmosphere and the ground allows to assess that, in the absence of any other heat transfer mechanism, the temperature of an ideal radiator in equilibrium with the sky could reach the value of the so called equivalent sky temperature or effective sky temperature, T_{sky}. (Perez-Garcia, 2004, p. 396)

T_{sky} can be defined by the relation to the dry bulb temperature written as (Perez-Garcia, 2004)

$$T_{sky} = \varepsilon^{1/4} T_{db} \quad (5)$$

where T_{db} is the dry bulb temperature in K and ε is the sky emissivity which is a function of the dew point temperature, T_{dp}, in ^{o}C. A definition for the dry bulb temperature is the temperature that is measured by a thermometer in a moist air environment. (Moran & Shapiro, 2004) In other

words, the air temperature people associate with when asking about the weather is the dry bulb temperature.

While Equation 5 is considered a standard, differences in defining the night sky temperature relate to the emissivity, ε. Multiple models exist for determining this value. Perez-Garcia takes four models and makes direct comparisons with experimental data in an attempt to determine the accuracy of each model. Of the four models presented, the model by Brunt proved to be the most accurate. (Perez-Garcia, 2004) However, the Brunt model relies on parameters that were calculated for different areas all over the world. Unfortunately these parameters were not given and they were not easily accessible. The three remaining models were fairly similar in their accuracy of determining the night sky temperature. So for the sake of simplicity, the model with the least amount of inputs was chosen. This model happened to be the one given by Berdahl and Fromberg in 1986. This model was also cited in a publication that discussed experiments of radiatively cooling a building using flat-plate solar collectors. (Erell & Etzion, 2000) It should be noted that the emissivity for both equations are for clear skies i.e. no clouds, dust, pollution etc. The emissivity for the night sky and day sky are

$$\varepsilon_{night} = 0.741 + 0.62\left(\frac{T_{dp}}{100}\right) \tag{6}$$

$$\varepsilon_{day} = 0.727 + 0.60\left(\frac{T_{dp}}{100}\right) \tag{7}$$

where T_{dp} is the dew point temperature in ^{o}C. (Perez-Garcia, 2004) The night sky emissivity will be used for the model to be calculated in this thesis, while the daytime equation can be neglected because all of the experiments will be run at night. However, if research of daytime cooling progresses, this would certainly be applicable.

INFRARED ANALYSIS

Sample Materials

The sample materials to be used as a potential cover for the radiator tested using the IR analysis were selected based on the general input from fellow engineers, curiosity for certain materials, and a general notion that some plastics are good for IR transmittance. Other factors that played into the sample selections were price and availability at the local hardware store. All samples were tested with both the IR camera and the FTIR spectrometer regardless of the results from the preliminary test with the IR camera. The materials selected can be seen in Table 2.

Table 2 *Materials selected for IR*

Material	Thickness [µm]	$/m^2
3M Transparency Film (sheets used for overhead projectors)	114.0	3.81
Typical glass slide	1016.0	28.71
Plexiglass (Non-glare Plaskolyte)	1270.0	38.75
Clear painter's sheeting [Polyethylene (PE)]	127.0	0.41
Polyvinyl chloride (PVC) (plastic wrap)	25.4	0.07
White trash bag (PE)	25.4	0.10
Black trash bag (PE)	63.5	0.10
Light switch plate (thermoset plastic)	16,510.0	36.37

Infrared Camera Overview

As stated previously, selecting potential cover materials to utilize in the experiments depended on two factors: cost and infrared transmissivity. To determine the infrared transmissivity, two tests were conducted. The first test involved using a FLIR ThermaCAM® S60 thermal infrared (IR) camera shown in *Figure 7* to quickly determine if materials selected showed any signs of having high transmission in the IR wavelengths of light.

Figure 7. FLIR ThermoCAM® S60 (American Infrared)

IR Camera Experimental Setup and Process

A cap with a diameter of 0.076 m and depth of 0.019 m was filled with water from the tap and placed in the microwave for 2 minutes on high. The resulting temperature of the water was hotter than the ambient and could easily be picked up by the IR camera. Many of the material samples were either not long enough or not strong enough to be able to lie across the cap, so a small holding template was made out of cardstock and placed on the lid. The setup can be seen in *Figure 8*. Each sample was placed on the setup and an infrared picture was taken.

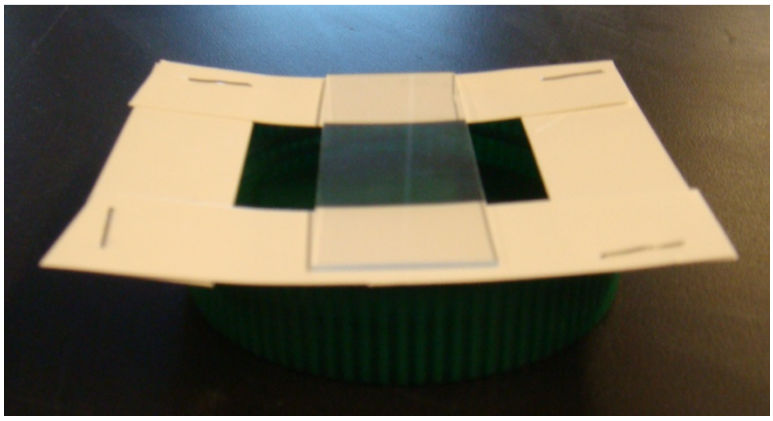

Figure 8. IR camera test setup with glass slide sample

IR Camera Results

The IR images that the camera provided showed that the PVC sample and the two different PE samples had the highest transmissivity. The captured images can be seen in *Figure 9*, *Figure 10*, and *Figure 11*. The square cutout of the cardstock can be seen due to the cardstock's

low transmissivity. The heated water is shown in a dark red to orange color while the area of the sample PVC and PEs can be seen because of its slightly lighter orange color. To contrast, the FLIR camera image of the glass slide sample can be seen in *Figure 12* which shows low transmission in the infrared light wave range.

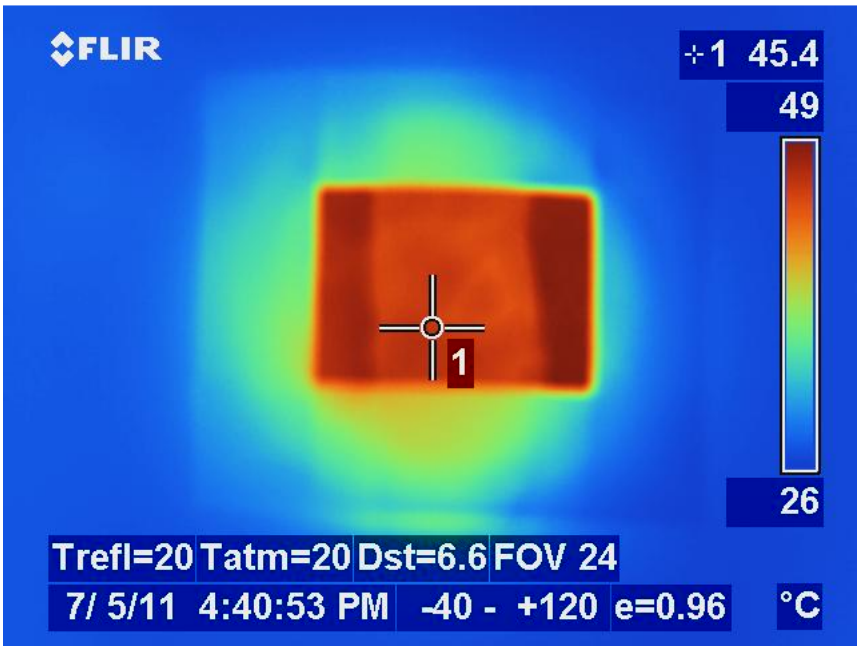

Figure 9. FLIR camera image of plastic wrap PVC

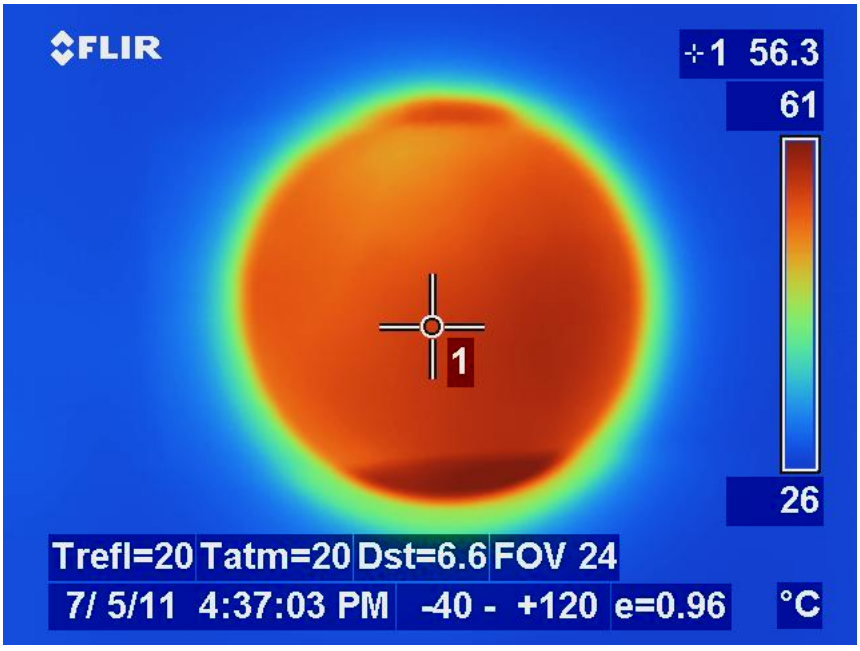

Figure 10. FLIR camera image of painter's roll polyethylene

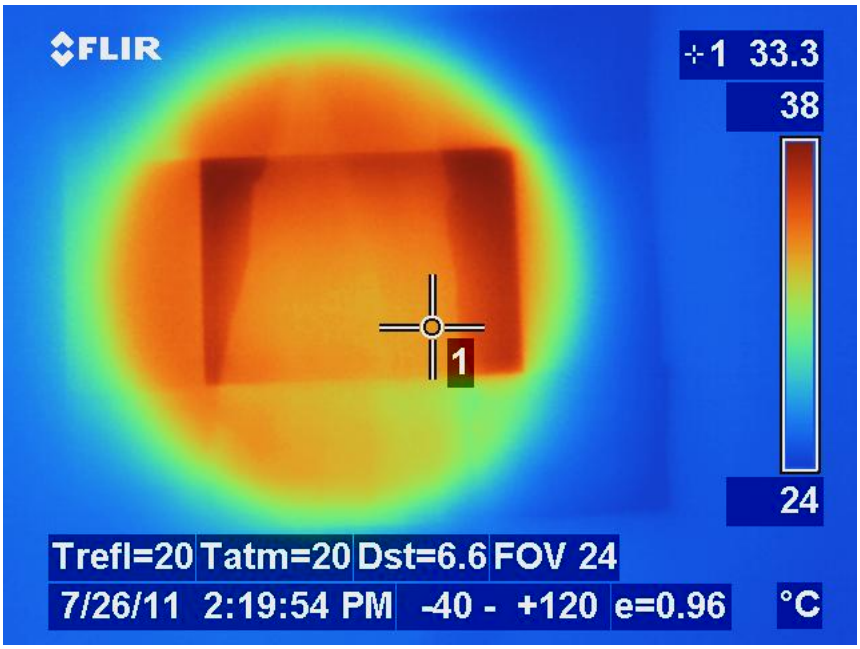

Figure 11. FLIR camera image of white trash bag polyethylene

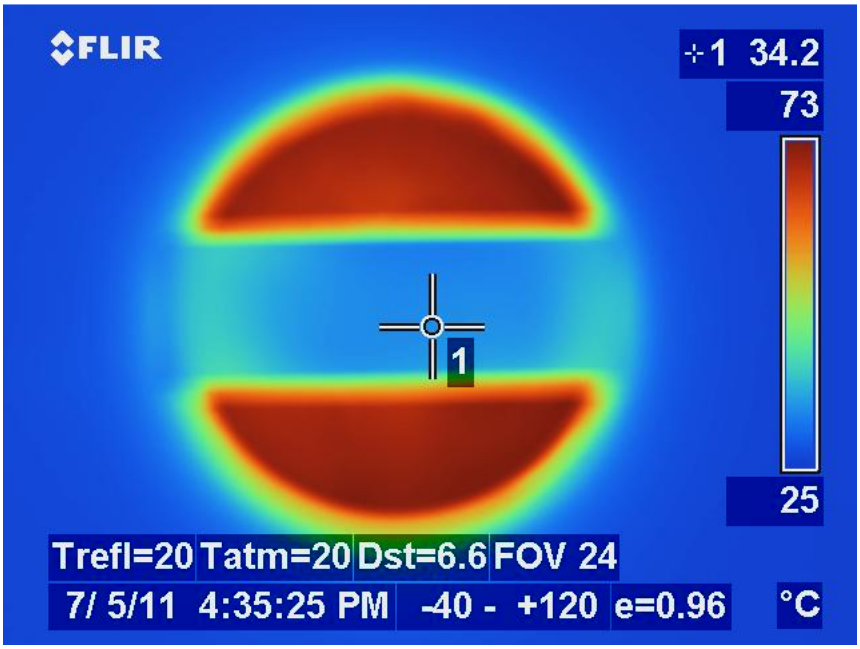

Figure 12. FLIR camera image of glass slide

FTIR Spectrometer

The cover material samples were analyzed on a Fourier Transform Infrared (FTIR) spectrometer with a wavelength range of 2.5 to 20 μm to determine IR properties, particularly % transmittance. The machine used was a Nicolet 6700 FT-IR spectrometer by the Thermo Electron

Corporation (Now Thermo Fisher Scientific). The spectrometer utilized the Smart Orbit which is a single-bounce diamond attenuated total reflection (ATR) accessory. ATR is a sampling tool that sends an IR beam of light into a crystal with a large index of refraction. The beam reflects from the inside of the crystal creating an evanescent wave. This wave enters the sample material that is laid on top of the crystal at a right angle. The evanescent wave loses some of its energy due to absorption of the sample material while the remaining energy of the wave is sent back to the detector. The signal at the detector can then be converted into meaningful data such as the depth of penetration. From this, absorbance and transmittance can be determined. (Technologies, 2010) A diagram of how ATR works with a sample can be seen in *Figure 13*.

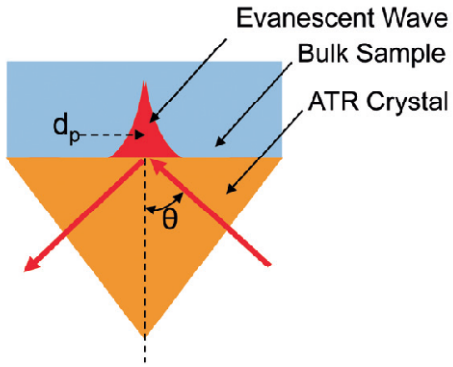

Figure 13. Diagram of an ATR evanescent wave (Technologies, 2010)

The FTIR spectrometer with Smart Orbit accessory can be seen in *Figure 14*. The product configuration for the accessory was for the Nicolet Avatar and Nicolet Nexus. Each sample was first cleaned with isopropyl alcohol and the plate was cleaned with methanol. To run the test, each sample was placed over the diamond crystal and held down with the pressure tower that was hand tightened.

Figure 14. Nicolet FTIR spectrometer with Smart Orbit accessory (Universitat Politecnica de Catalunya - Barcelona Tech, 2011)

The software the spectrometer used was Thermo Scientific's Omnic package. The software required minimal setup. Some important settings chosen were the following: using 64 scans, outputting the data in terms of % transmittance, and using a gain of 2. The 64 scans were chosen due to unfamiliarity with the machine. Sixteen scans would have been enough to gather a reading of the material. The gain of two was the default setting. All other settings were kept at the default settings. Before testing each sample, a background was collected. This allowed for the machine to compute the % transmittance from the material and then display it in the correct terms. Each sample was tested three times using three different locations on the sample to provide an average set of data.

FTIR Results

The software provided a result for each test plotting the wavenumber, cm^{-1}, (x-axis) against % transmittance (y-axis). The data was transferred to Microsoft Excel and the wavenumber, η, was converted to wavelength, μm, using the formula found in Equation 8. An updated plot was then created.

$$\lambda = 10000/\eta \tag{8}$$

The FTIR machine provided data to determine, more specifically, what materials were suitable to test as cover materials. *Figure 15* shows the FTIR results for clear polyethylene painter's sheeting, a white polyethylene trash bag, and PVC plastic wrap. All three of these samples proved to be very transparent in the desired wavelength range, with the two polyethylene samples having a higher % transmittance between 8 and 14 μm.

It should be noted each set of data is an average of three samples from the FTIR spectrometer. Each sample was tested three times to display slight differences in testing conditions due to the inability to apply the same amount of pressure with the clamp on the sample each time.

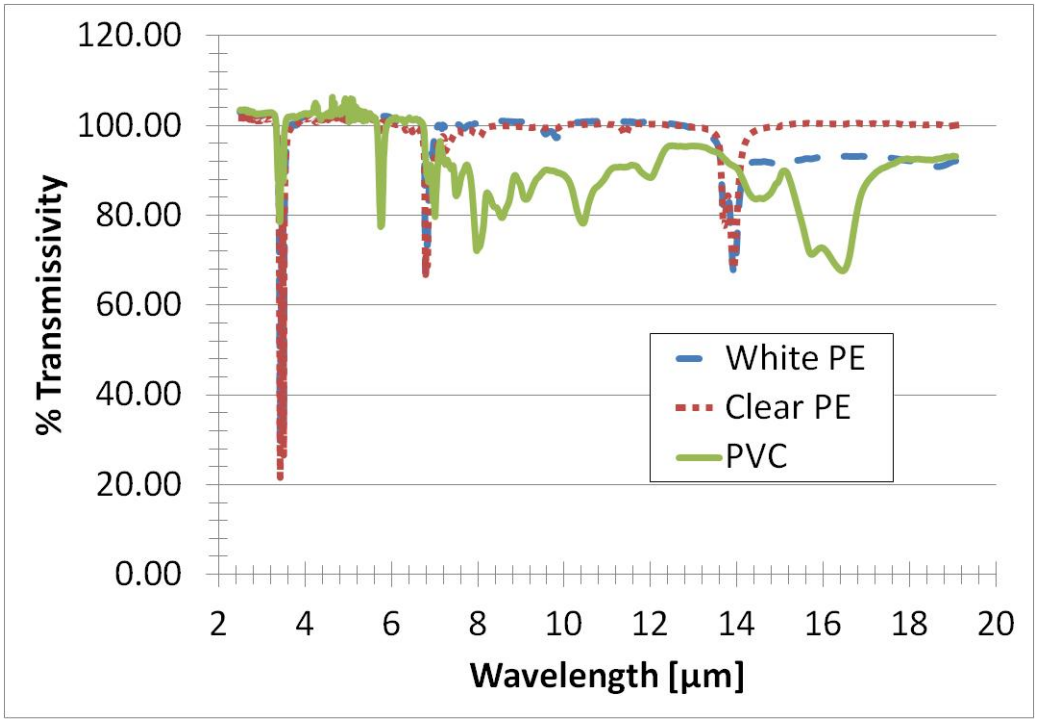

Figure 15. Selected materials from FTIR analysis

Extinction Coefficients

The data from the FTIR spectrometer was used to calculate extinction coefficients for the material tested. This was useful because once an extinction coefficient is determined, the transmittance no longer only applies to a certain thickness, but can be calculated at varying thicknesses. For simplicity, Beer's Law was applied to determine the extinction coefficients. Beer's Law is written as

$$\tau_\eta = e^{-\kappa_\eta s} \tag{9}$$

where τ_η is the transmittance, s is the thickness of the material and κ_η is the extinction coefficient. The subscript, η, denotes that it is a function of the wavenumber. (Modest, 2003) This can easily be converted to wavelength by simply taking the reciprocal of the wavenumber.

To find the extinction coefficients, both values for the thickness and transmissivity were needed. The transmissivity values for the range of wavelengths were taken from the FTIR data. The thickness was found using equations from attenuated total reflection spectroscopy theory. This calculated thickness is called the effective path length (EPL). (Averett, Griffiths, & Nishikida, 2008) Calculating the EPL requires looking at the effect of polarization on the measurement from the FTIR spectrometer and therefore is dependent on certain properties of the machine and setup. The effect of polarization is split into two separate equations which are

$$d_{e,s} = \frac{n_{21}\lambda_o cos\theta}{n_1\pi(1-{n_{21}}^2)(sin^2\theta-{n_{21}}^2)^{1/2}} \tag{10}$$

$$d_{e,p} = \frac{n_{21}\lambda_o cos\theta(2sin^2\theta-{n_{21}}^2)}{n_1\pi(1-{n_{21}}^2)[(1+{n_{21}}^2)sin^2\theta-{n_{21}}^2](sin^2\theta-{n_{21}}^2)^{1/2}} \tag{11}$$

where $d_{e,s}$ is the effective thickness for perpendicular polarization, $d_{e,p}$ is the effective thickness for parallel polarization, n_{21} is the ratio of the indices of refraction (n_2/n_1), λ_o is the wavelength in a vacuum, θ is the angle of incidence of the inner surface of the diamond crystal, n_1 is the refractive index of the diamond crystal and n_2 is the refractive index of the sample. (Harrick & du Pre, 1966) The effective penetration is calculated as

$$d_e = \frac{d_{e,s}+d_{e,s}}{2} \tag{12}$$

Finally the EPL is given by

$$EPL = N \times d_e \tag{13}$$

where N is the number of reflections or bounces in the diamond crystal. This EPL is then paired with its respective wavelength in a vacuum, λ_o, and entered into Beer's Law from Equation 9. (Technologies, 2010)

The data from the FTIR was used to determine extinction coefficients for the PVC, white PE and clear PE. It should be noted that the amplitude on the original data from the machine is not accurate. Looking back at *Figure 15*, the % Transmittance is actually higher than 100% at certain wavelengths. This is the result of a focusing error within the machine where too much light is reflected back into the detector due to a diverging parallel beam causing it to register a higher intensity of light than is actually occurring. (Young) To account for this, a modification to the data was made. The highest transmittance value was determined for each material. If that value was higher than 1, the difference between the value and 1 was determined. That difference value was then subtracted from the other transmittances leaving the highest transmittance at a value of 1. The modified transmittances were used in the Beer's Law equation to calculate the extinction coefficients.

A plot of the extinction coefficients for the PVC, clear PE and white PE can be seen in *Figure 16*. Once the extinction coefficients were known, the transmittance at all wavelengths was calculated using the thickness of the material. The thicknesses for the materials used for this thesis can be found in Table 2. The actual transmittance for the materials can be seen in *Figure 17*. From this figure, it can be seen that the best option is the white polyethylene cover. While it has relatively the same extinction coefficients as the clear polyethylene, it's thickness of only 25.4 µm makes it more transmissive than the 101.6 µm clear PE. The PVC is not appropriate for this experiment because of its higher extinction coefficients and therefore, a lower transmittance. It should be noted that each material shows an emissivity of 1 at some point in the plot i.e. the clear PE has a transmittance of 1 between a wavelength of 4 and 5 µm. This is due to the amplitude error in the machine measurement as well as the modification that was made to the data.

As *Figure 17* shows, the white polyethylene has the highest transmittance on average for the three materials. More specifically, it has a value around 0.9 between the wavelengths of 8 and 13 µm. Therefore, the value for the transmittance of the cover in the model will be taken as 0.9.

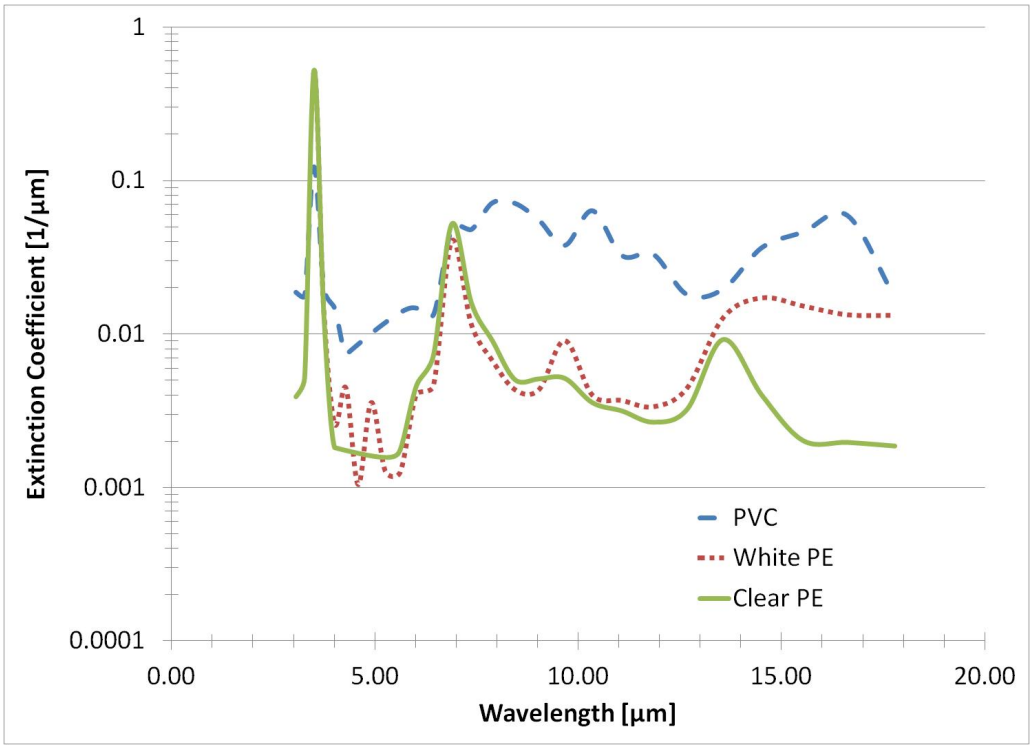

Figure 16. Extinction Coefficients of selected materials

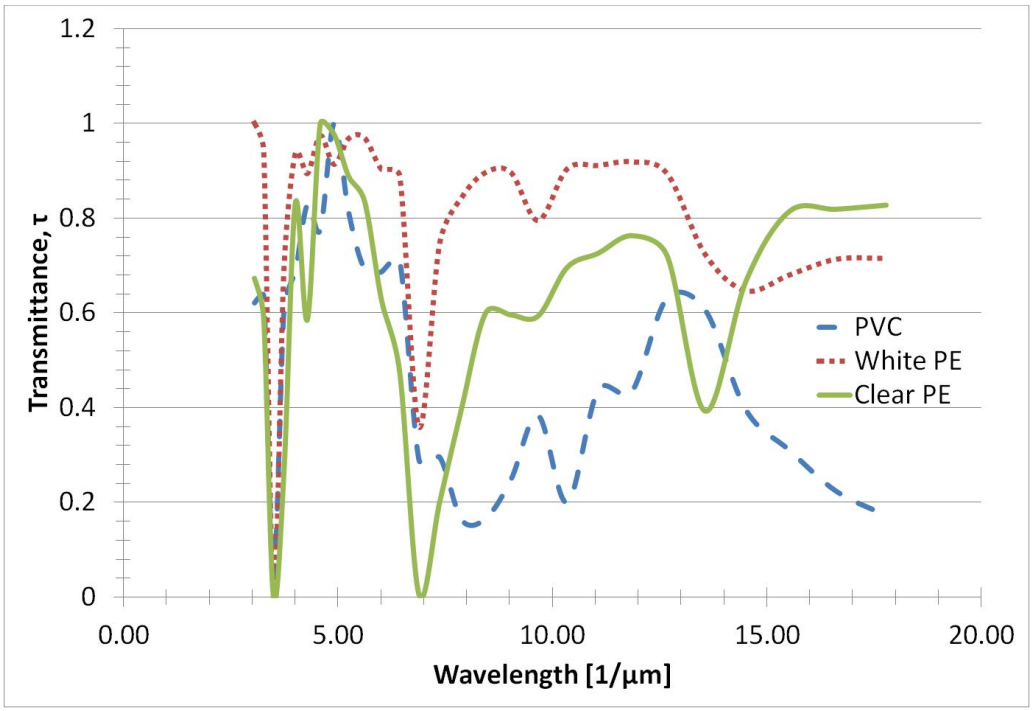

Figure 17. Transmittance of selected materials with given thickness in Table 2

RADIATIVE COOLING EXPERIMENTAL SETUP

Date & Location

The experiments took place between August and November of 2011. The experiments were run on the rooftop of the Engineering Center F Wing on the Tempe Campus at Arizona State University. It should be noted that there were many objects and buildings in the surrounding area and in the radiator field of view that could affect the radiative emission from the water and they will be discussed later. *Figure 18* shows the layout of the rooftop and where the different experiments were placed. The reason that the experiments were in different locations was because of the size of the setup and the proximity to an outlet for power. The tray experiment was run further away from the small room because the trays took up much more space than the glass containers. Also, the location of the tray experiments helped reduce the shape factors of the objects on the rooftop. This was not considered as much of an issue with the glass containers because it was only for validation.

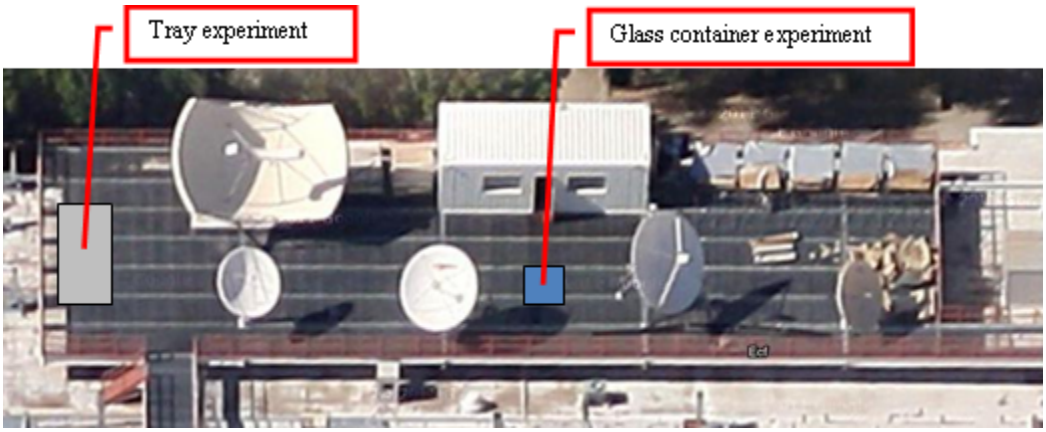

Figure 18. Experiment Location

Micrologger and Thermocouples

A Campbell Scientific CR23X: Micrologger® for Data Acquisition was used to measure the temperatures of the water in the various containers as well as the ambient air. Data collection was performed by using the program PC200W version 4.1. This software allows the user to monitor data in real time and collect data for further analysis with other software. A Gigaware® USB-A to Serial DB9 connector was used to connect the CR23X Micrologger to a laptop

computer. Five total thermocouples were used in the experiment. The CR23X Micrologger setup can be seen in *Figure 19*.

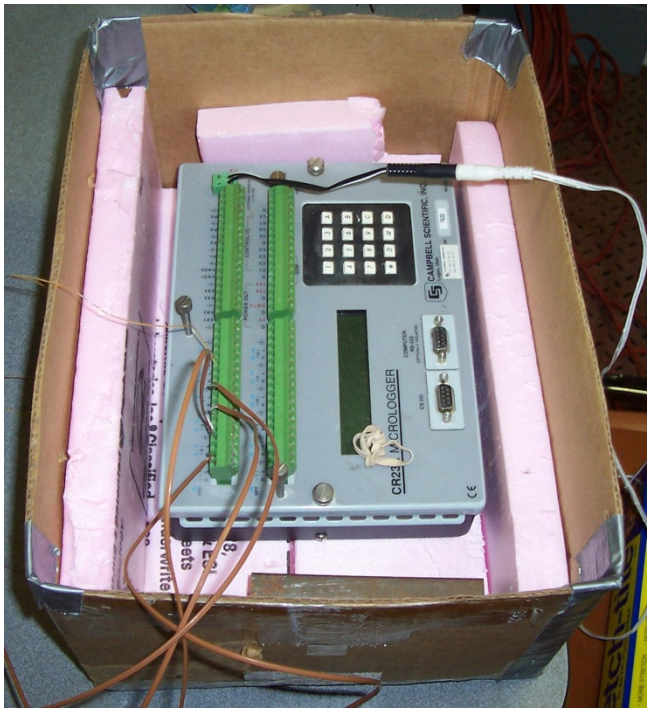

Figure 19. CR23X Micrologger® for Data Acquisition with attached thermocouples

Four Omega hermetically sealed tip insulated thermocouples were used for obtaining the temperature of the various water samples. Three of those thermocouples were type J and the other was type K. The thermocouples were 24 AWG stranded and 1 m in length. Two different types were used due to the limited supply of these thermocouples in the lab. The thermocouples were calibrated using the CR23X Micrologger while being submerged in ice water. The temperatures displayed were compared with the temperature measurement from a -5 ^{o}C to 30 ^{o}C Immersion Thermometer by the Kessler Thermometer Corporation. The results showed that the thermocouples were only off by a maximum of 0.2 ^{o}C. Originally, the ambient air temperature was measured using the reference temperature from the CR23X Micrologger. But after a couple nights of data collection, this temperature was noticeably lower than recorded temperatures from weather stations around the area. This data was thrown out and the ambient air temperature was then measured using a typical insulated type K thermocouple with an exposed junction, which produced much more accurate results. This thermocouple was also calibrated in ice water with the

CR23X Micrologger and immersion thermometer. During the experiment, data was recorded every two seconds. This data was then averaged for a period of one minute. The output data was given in temperature every one minute.

Vacuum Insulated Glass (VIG)

The experiment involved different vacuum insulated glass (VIG) inserts. The original idea came from the concept of a large Dewar flask. This would eliminate the need to insulate the sides. Because Dewar flasks are very expensive, older commercial vacuum flasks were the next alternative. Unfortunately, due to vacuum flasks being out of date and relatively hard to find, six different flasks were purchased but consisted of four different types. This was considered to be acceptable due to the fact that this experiment was only used as a verification test for the larger tray experiment.

The first round of testing used two Aladdin® VIC 020A fillers and two Thermos® VIC 70F fillers. The dimensions for these containers as well as containers used in latter experiments can be seen in Table 3. The containers were placed in holes cut out in extruded polystyrene and placed in a cardboard box as shown in *Figure 20*.

Table 3 *Container radiation areas and water volumes*

Container	020A	040A	70F	72F	Tray: clear PE	Tray: white PE
area [m^2]	$2.819x10^{-3}$	$5.076x10^{-3}$	$4.774x10^{-3}$	$4.576x10^{-3}$	0.344	0.344
volume of water [m^3]	$2.5x10^{-4}$	$3.7x10^{-4}$	$3.0x10^{-4}$	$3.7x10^{-4}$	$1.2x10^{-2}$	$1.7x10^{-2}$

Figure 20. Initial setup with 020A VIG fillers (foreground) and 70F VIG fillers (background)

The top portions of the containers were wrapped with reflective bubble wrap insulation so that no glass was left exposed to the open air. The 020A VIG containers were filled with 250 mL of water while the 70F containers were filled with 300 mL of water. This left a distance of 2 and 3 inches of air between the water and the tops of the 020A and 70F containers, respectively. The containers were covered with clear 4 mil (~100 microns) polyethylene painter's sheeting. To keep the polyethylene attached, rubber bands were placed around the covers. The wrinkles were smoothed out so that the water had a clear path to radiate to the sky. Also shown in *Figure 20* are the thermocouples. They were placed in the water by being bent over the edge of the container and held down by the rubber band around the cover material.

This setup was run multiple times with two different main conditions. The first round of experimenting started with water that was well below ambient temperature at the beginning of the process. The water in the containers was kept in a room with an average temperature of 27 degrees Celsius while ambient was 37 degrees Celsius or higher. The second experimental condition was having the water in the containers start at ambient temperature. This was done by placing the test setup outside with a piece of cardboard covering the containers to prevent incoming radiation from

heating the water up or letting heat escape via radiation and cool the water down. The cover was then removed when the temperatures of the water were even with the ambient temperature.

The next setup for the VIG containers involved plastic wrap to verify the results from the FTIR analysis. One of the 020A containers had the clear polyethylene removed and was replaced with clear plastic wrap made of polyvinyl chloride (PVC). The tests run utilized all four containers, with the other three remaining the same as before. The next series of tests involved larger VIG 72F filler and medium sized 040A filler. Both of these containers were filled with approximately 370 mL which left a gap of approximately 2 and 3 inches from the top rim for the medium and large containers, respectively. Both of these containers were covered with clear polyethylene. Another setup replaced the clear polyethylene cover with white polyethylene taken from a trash bag. The white polyethylene covered the 040A container.

The overall goal of this experiment was to gain a sense of how successful an actual tray radiator may be at radiating heat to the night sky. The small containers were given different initial conditions to determine if, one, the water could be cooled below ambient temperature by radiation on a small scale, and two, to determine if different initial conditions affected the experiment in any way. It will be seen that the results of these experiments justified continuing the project by scaling up the size of the radiators and simulating more closely the design of a potential commercial radiator.

Tray Experiment

Earlier in this thesis, it was noted that one way to increase the rate of radiative heat transfer is to increase the area being cooled. The VIG containers have a radiation view area of approximately 45.2 cm^2 for the 70F, 72F and 040A containers, while the 020A containers have a radiation view area of approximately 30 cm^2. Presumably, the experiments should scale up for radiators with larger areas. In order to provide experimental data to back this claim up, two fiberglass trays with a depth of approximately 2 inches and a total area of 0.344 m^2 were modified into night sky radiators. A modified tray can be seen in *Figure 21* and a diagram of the entire tray system can be seen in *Figure 22*. On each of the shorter ends of both trays, a small hole with diameter ~ 6 mm was drilled and an aluminum tube was fitted and bent up so that the top of the

tube was higher than the rim of the tray. This was done to provide a way to submerge the thermocouples in the water without having to seal them to the fiberglass. Another hole of diameter ~ 2.5 cm was drilled to fit a PVC pipe on the same end as one of the aluminum tubes. This was built in for an easy access point to fill the system with water. The two aluminum tubes and PVC pipe were attached to the fiberglass tray using Loctite® Professional Heavy Duty Epoxy. Each tube and pipe was also sealed with Polyseamseal ® Speed Seal Silicone Sealant to prevent water leaking through any holes not completely covered with the epoxy.

Figure 21. Tray night sky radiator with white polyethylene cover

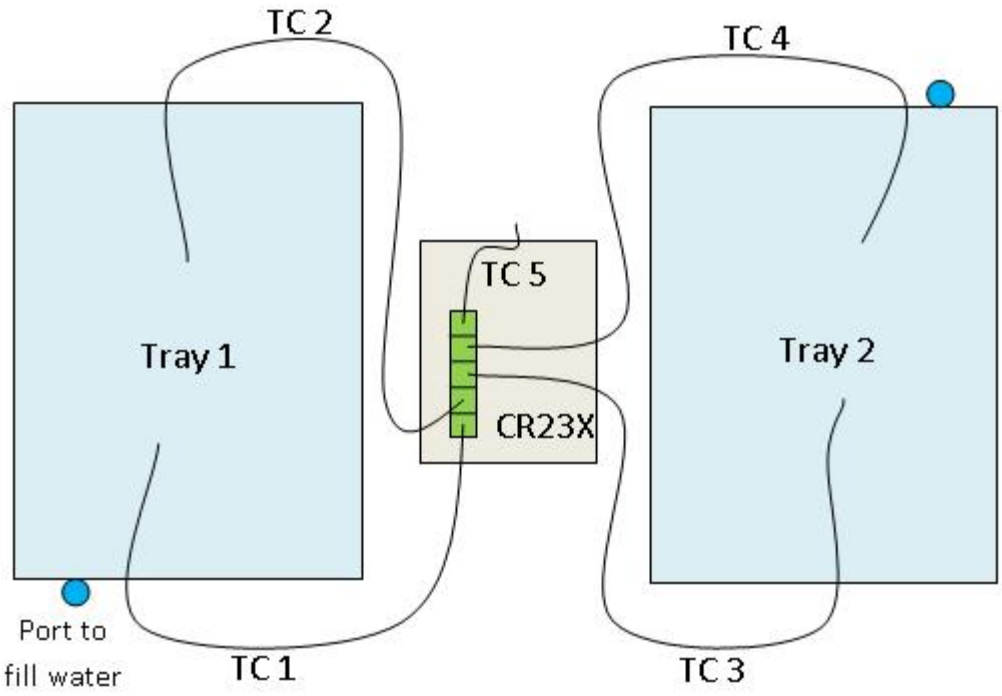

Figure 22. Diagram of tray experiment setup

Each tray received a different cover. One tray was covered with the clear polyethylene painter's sheet with a thickness of 101 microns. The other tray was covered with white polyethylene from a trash bag with a thickness of 25 microns. Polyethylene is extremely difficult to bond to other materials. To achieve this, 3M® Hi-Strength 90 Spray Adhesive was used because it's specifically designed for plastics. Finally, insulation was added to the trays to reduce the effect of convection. Two layers of one inch thick extruded polystyrene were added on the bottom surface of the trays. The outer walls were then covered with two layers of reflective insulating bubble wrap. Both the polystyrene and bubble wrap were attached using ACE® Carpet Tape Fiberglass and duct tape.

Once the trays were fully modified, they were filled with water. Each tray was filled with 18 liters of water, but this changed due to leaking in the system. The white PE tray was estimated to have 17 liters while the clear PE tray was estimated to have 12 liters. The trays were filled up near the top of the rim, but a 0.01 m space was left for air to act as a barrier. It should be noted that the cover was not even with the edge of the tray, but higher due to the flexible nature of the plastic

and the pressure from the air sitting on top of the water. The same thermocouples and CR23X Micrologger were used to take measurements. Each tray utilized two thermocouples placed at approximately the one third and two third marks on the tray to give a better idea of the overall temperature of the water. The setup for this experiment can be seen in *Figure 23*. A simple variation was run with this setup as well. In order to see how much of an effect convection had on the system, the experiment was run multiple times where the tray with the clear polyethylene was covered with an opaque white poster board. This was to effectively eliminate the heat loss from the system due to radiation. The last experiment involving these trays compared an aluminum cover to the white polyethylene cover to determine if the direct fluid emission system can compete with the conventional system. The aluminum radiator was made by removing the clear polyethylene from the other tray and adhering aluminum foil to the tray.

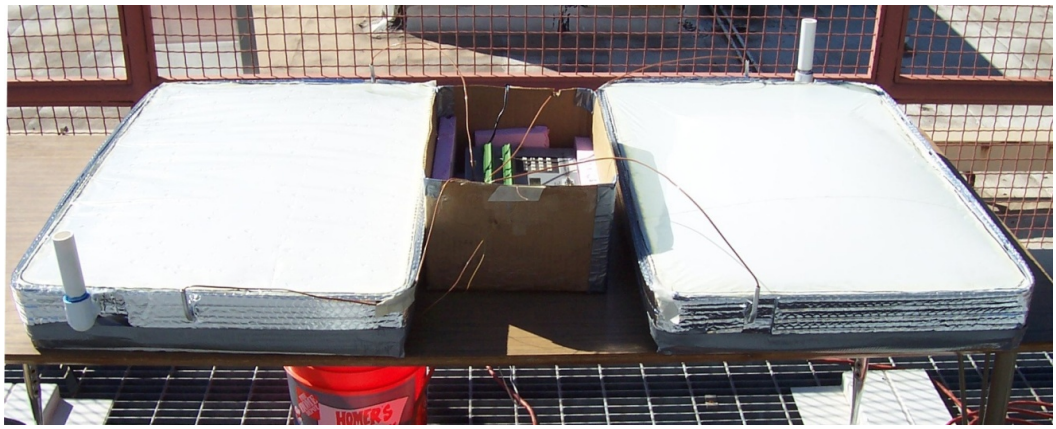

Figure 23. Tray experiment setup

MODEL

A model was created to theoretically determine the effective cooling power of the radiator. The model was designed after the tray experiment using its dimensions as well as the same materials and their properties. A diagram of this model as a resistance network can be seen in *Figure 24*. This diagram can be expressed by the equation

$$\sum q = q_{rad,w\ to\ sky} + q_{rad,w\ to\ \infty} + q_{rad,w\ to\ cover} + q_{top,R} + q_{side,R} + q_{bottom,R} \tag{14}$$

where $q_{rad,w\ to\ sky}$ is the radiation from the water to the sky, $q_{rad,w\ to\ \infty}$ is the radiation from the water to the surroundings, $q_{rad,w\ to\ cover}$ is the radiation from the water to the cover, $q_{top,R}$ is the heat flux calculated from the resistance network of the conduction through the air gap, convection from the cover to the surroundings, and the radiation of the cover to the surroundings, $q_{side,R}$ is the heat flux from the resistance network of convection and conduction through the sides, and $q_{bottom,R}$ is the heat flux from the resistance network of convection and conduction through the bottom. The radiation from the water to the cover can be neglected due to the very small difference in temperature.

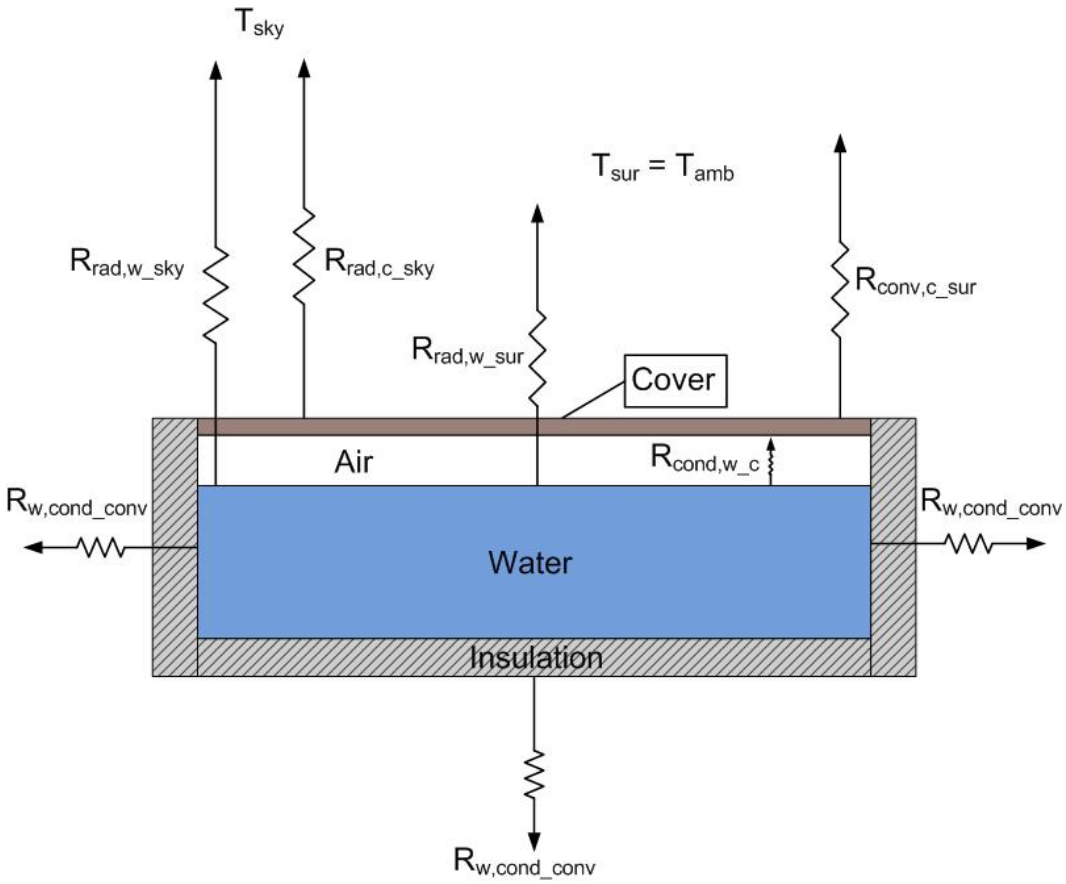

Figure 24. Diagram of the radiator model as a resistance network

The model consists of 17 L of water inside the tray with dimensions of 0.727 m by 0.473 m for a total area of 0.344 m. The tray was 0.048 m high. The insulation on the bottom consisted of 0.0508 m polystyrene with a conductive resistance, R_{cond}, of 4.168 KW^{-1} and a convective resistance, R_{conv}, of 0.524 KW^{-1}. The insulation on the sides consists of bubble wrap 0.0159 m thick with R_{cond} of 0.640 KW^{-1} and R_{conv} of 6.369 KW^{-1}. The air gap in between the water and the cover is considered to be 0.01 m. Because it is impossible to have forced convection between the cover and water, free convection was considered. With some analysis using the Rayleigh number and Nusselt number, it can be seen that the air acts as a conductor with a thermal conductivity, *k*, given for the appropriate temperature. It should be noted that because the temperature range from the experiment was from 300 K to 280 K, an average temperature of air was used to determine appropriate values. That temperature was 293 K (20^{o}C) for simplicity. This was done only after checking the equations, utilizing associated values to this temperature, with higher and lower

temperatures and seeing that the effect of using an average temperature was minimal. From the temperature of 293 K, the following values were used for air: density, ρ = 1.204 kgm^{-3}, dynamic viscosity, μ = 1.825*10^{-5} $kgm^{-1}s^{-1}$, thermal conductivity, k = 0.02514 $Wm^{-1}K^{-1}$, and Prandtl number, Pr = 0.7308. (Çengel, 2007) The water also has an emissivity of 0.96. (Modest, 2003) Finally, the cover was assumed to be polyethylene with a thickness of 25.4 μm, an emissivity of 0.1, and a transmissivity of 0.9 from the FTIR analysis.

It was assumed that the water can be taken as a lumped mass where the temperature is constant throughout. The experimental results can verify that the difference in temperature across the water was rarely more than 0.5 ^{o}C. From this lumped capacitance model, a resistance network was setup up to determine the heat moving in and out of the system. Resistance networks utilize the following equation:

$$q = \frac{\Delta T}{\Sigma R} \tag{15}$$

where ΣR is the sum of the resistances of each mode of heat transfer. The first term found was the heat transferred to the sky via radiation from the water written as

$$q_{rad,w\_sky} = \sigma \varepsilon \tau A (T_w^4 - T_{sky}^4) \tag{16}$$

where σ is the Stefan-Boltzmann constant, ε is the emissivity of the water, τ is the transmissivity of the cover, A is the area of the water being radiated, T_w is the temperature of the water, and T_{sky} is the same from the model mentioned in the Sky Temperature section of the thesis. Along with radiating to the sky, the water also radiates to the surrounding area which was assumed to have a temperature equal to the ambient temperature. This expression is

$$q_{rad,w\_sur} = \sigma \varepsilon \tau A F (T_w^4 - T_{sur}^4) \tag{17}$$

where T_{sur} is the temperature of the surrounding area and F is the shape factor computed by analyzing the buildings and objects in the area. It should be noted that the temperature of the surrounding objects were assumed to be the same as the ambient temperature and may therefore be also written as T_∞. F is determine by using the equation

$$F_{d1-2} = \frac{1}{2\pi}\left(tan^{-1}\frac{1}{Y} - \frac{Y}{\sqrt{X^2 + Y^2}} tan^{-1}\frac{1}{\sqrt{X^2 + Y^2}}\right) \tag{18}$$

where F is the shape factor, $Y = a/c$ and $X = c/b$ with a as the height, b as the width and c as the distance from the object. (Modest, 2003)

The cover also radiates to the sky and is represented by

$$q_{rad,c\_sky} = \sigma \varepsilon_{cover} A(T_c^4 - T_{sky}^4) \tag{19}$$

where T_c is the temperature of the cover. Its radiation to the surrounding objects can be neglected because the temperature difference and emissivity are very small. The terms for the conduction of the water across the air to the cover, the conduction across the cover, and the convection from the cover were lumped together in a resistance analysis written as

$$q_{cond,cover} = \frac{T_w - T_{sur}}{\left(\frac{1}{h_a A} + \frac{L_c}{k_c A} + \frac{L_a}{k_a A}\right)} \tag{20}$$

where h_a is the heat transfer coefficient of the air, L_c is the thickness of the cover, k_c is the thermal conductivity of the cover, L_a is the characteristic length of the surface going through convection (L_a = area/perimeter), and k_a is the thermal conductivity of air. The h_a term was found by assuming a value of 4.95 ms^{-1} for a wind speed taken from TMY3 data and finding the Reynold's number which is

$$Re = \frac{\rho u_\infty x}{\mu} \tag{21}$$

where Re is the Reynold's number, u_∞ is the wind speed, x is the critical length, and μ is the dynamic viscosity. From this equation, the Nusselt number can be found using

$$\overline{Nu} = 2Nu = 0.664 Re^{1/2} Pr^{1/3} \tag{22}$$

where $\overline{Nu}$ is the average Nusselt number and Nu is the Nusselt Number. Finally, the Nussult number can be plugged into the equation

$$Nu = \frac{hx}{k} \tag{23}$$

Solving for h then gives h_a. This process is the same for finding the heat transfer coefficient for the sides and bottom of the radiator as well. Coupling the conductive and convective resistances together gives the heat rate, q, for both the sides and bottom, respectively.

Finally the heat rates are totaled and set equal to the heat stored in the system shown by

$$\Sigma q = \rho V c_p \frac{\Delta T}{\Delta t} \tag{24}$$

where V is the volume of water, c_p is the specific heat of water, ΔT is the change in temperature of the water, and Δt is the time difference between each step. To find the new temperature of the water ΔT breaks up into

$$\Delta T = T_{w,old} - T_{w,new} \tag{25}$$

where $T_{w,old}$ is the original temperature of the water and $T_{w,new}$ is the newly computed temperature of the water. The process was run with a Δt = 300 s over a 14 hour period. Heat rates, q, were calculated for each 300 s time step. A 300 s time interval was considered adequate because the ASU weather station data is given hourly, therefore the 5 minute data is interpolated and not entirely accurate with the 5 minute actual real time temperature data.

The entire equation used for the model can be written as

$$\begin{aligned} &\rho V c_p \frac{T_{w,old} - T_{w,new}}{\Delta t} \\ &= \sigma \varepsilon_w \tau_{cover} A_{top} \left(T_w - T_{sky}\right) + \sigma \varepsilon_w \tau_{cover} A_{top} F (T_w - T_\infty) \\ &+ \frac{T_w - T_\infty}{R_{top,cond,air} + R_{top,cond,cover} + R_{top,conv,air} + R_{top,rad,cover}} \\ &+ \frac{T_w - T_\infty}{R_{sides,cond,fb} + R_{sides,cond,wrap} + R_{sides,conv,air}} \\ &+ \frac{T_w - T_\infty}{R_{bottom,cond,fb} + R_{bottom,cond,foam} + R_{bottom,conv,air}} \end{aligned} \tag{26}$$

The final result for the model can be seen in *Figure 25*. The plot shows the dry bulb temperature, the temperature change of the water, the heat transfer rate, and the sky temperature. The dry bulb temperature and dew point temperature used to calculate the sky temperature were taken from the ASU weather station data center. The data used was from October 28th through the 29th between 6 PM and 8 AM. The heat flux at the crossover point (point when q_{conv} and q_{cond} = 0)

is 76.67 Wm^{-2} and occurs at 2:55 AM and the radiator efficiency (actual $q_{rad,total}$ divided by $q_{rad,ideal}$) at this point is 0.92.

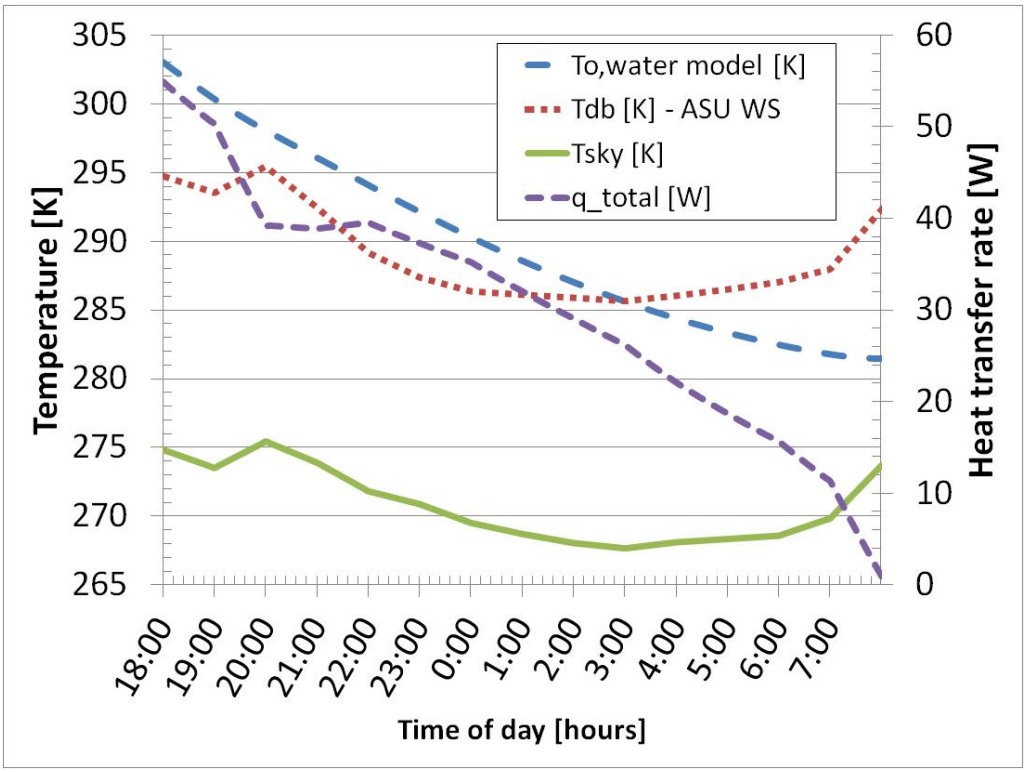

Figure 25. Theoretical model using ASU weather station temperature data from 10/28-29/2011

EXPERIMENTAL RESULTS

Metric for Analysis

To be able to compare the results from the conducted experiments, the data collected needed to be converted to a common metric. A useful metric for this comparison is measuring the heat flux per unit area. This will also allow an easy comparison with the data reported in other experiments as well. Because the system is not flowing, the only energy contained in the system is the energy stored, or the heat stored which can be written as

$$\dot{E}_{st} = \dot{q}_{st} \tag{27}$$

where $\dot{E}_{st}$ represents the energy stored and $\dot{q}_{st}$ represents the heat stored. This will be the starting point. From here, the heat stored can be represented as

$$q_{st} = \rho c_p \frac{\partial T}{\partial t} dxdydz \tag{28}$$

where ρ is the density, c_p is the specific heat, $\frac{\partial T}{\partial t}$ is the time dependent temperature differential, and *dxdydz* is the combination differential of each direction. (Incropera, Dewitt, Bergman, & Lavine, 2007) Because the volume will not be changing

$$V = dxdydz \tag{29}$$

where *V* is the volume. Plugging this back into the heat stored equation gives

$$q_{st} = \rho V c_p \frac{\partial T}{\partial t} \tag{30}$$

The temperature and time used for the analysis are simply the starting and ending temperatures for each increment which results in

$$q_{st} = \rho V c_p \frac{T_{w,old} - T_{w,new}}{\Delta t} \tag{31}$$

where ΔT is the difference in temperature and Δt is the difference in time. Finally, the heat stored term can be divided by the area to give the heat rate in terms of energy per unit area or Wm^{-2} giving

$$q" = \frac{\rho V c_p}{A} \frac{T_{w,old} - T_{w,new}}{\Delta t} \tag{32}$$

where A is the area of the surface that is radiating heat. This q'' is the total heat flux of the system which takes into account radiation, convection and conduction. Because q'' is not just the heat flux due to radiation, a specific value of the data will be looked. This value is the crossover value which is the point when the temperature of the water is the same as the temperature of the ambient air. At this point, the difference in temperature is zero and therefore the heat flux can only be a result of radiation.

For the following results, the density of water, ρ, was taken to be 1000 kgm^{-3} and the specific heat of water was taken to be 4181 $Jkg^{-1}K^{-1}$. The areas of the containers and volume of water are also needed to be able to perform the calculations. These can be seen in Table 3.

It should be noted that the heat flux values were calculated by averaging the one minute interval values. This interval was used because it was the interval that the CR23X Micrologger retrieved data. It contrasts to the model because the model uses 5 minute intervals of data. While the model could have used one minute intervals, it was unnecessary because the temperature data from the ASU Weather Station was only recorded on an hourly basis and therefore interpolation to 1 minute instead of 5 minutes would lead to the similar values for the heat flux.

The tray experimental results make a comparison with the ideal heat flux due to radiation. This equation is

$$q_{rad,ideal} = \sigma\varepsilon({T_w}^4 - {T_{sky}}^4) \tag{33}$$

where the emissivity, ε, is for water. The experimental results are divided by the ideal radiation heat flux to give a radiation efficiency.

VIG Results

This test was run multiple times to gather data for different initial conditions. The different initial conditions were having the water temperature initially warmer than the ambient temperature, the water temperature about equivalent to the ambient temperature, and the water temperature cooler than the ambient temperature. All of these data presented is from experiments that used clear PE which was considered the best because of durability.

The experiment shown in *Figure 26* had the initial condition of the ambient temperature being higher than the water temperature. The data shown reflects water from a 70F container. The heat flux was calculated to be 33.7 Wm^{-2} by averaging the one minute data over the entire period. This heat flux can only be from the effect of radiation because any other heat transfer mechanisms would have increased the temperature of the water.

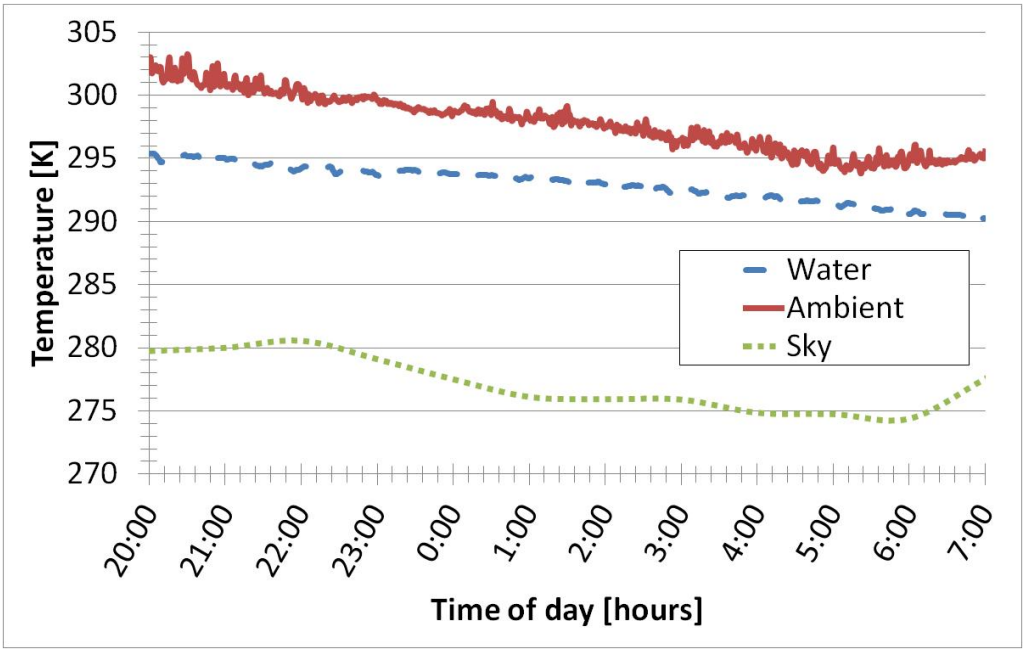

Figure 26. VIG experimental data from 9/18-19/2011 where initial ambient temp > water temp

The experiment shown in Figure 27 had the initial condition of the ambient temperature being almost equal to the initial temperature of the water. The data shown is from a 70F container. The heat flux for this experiment is 86.4 Wm^{-2}, a figure much higher than the first experiment discussed.

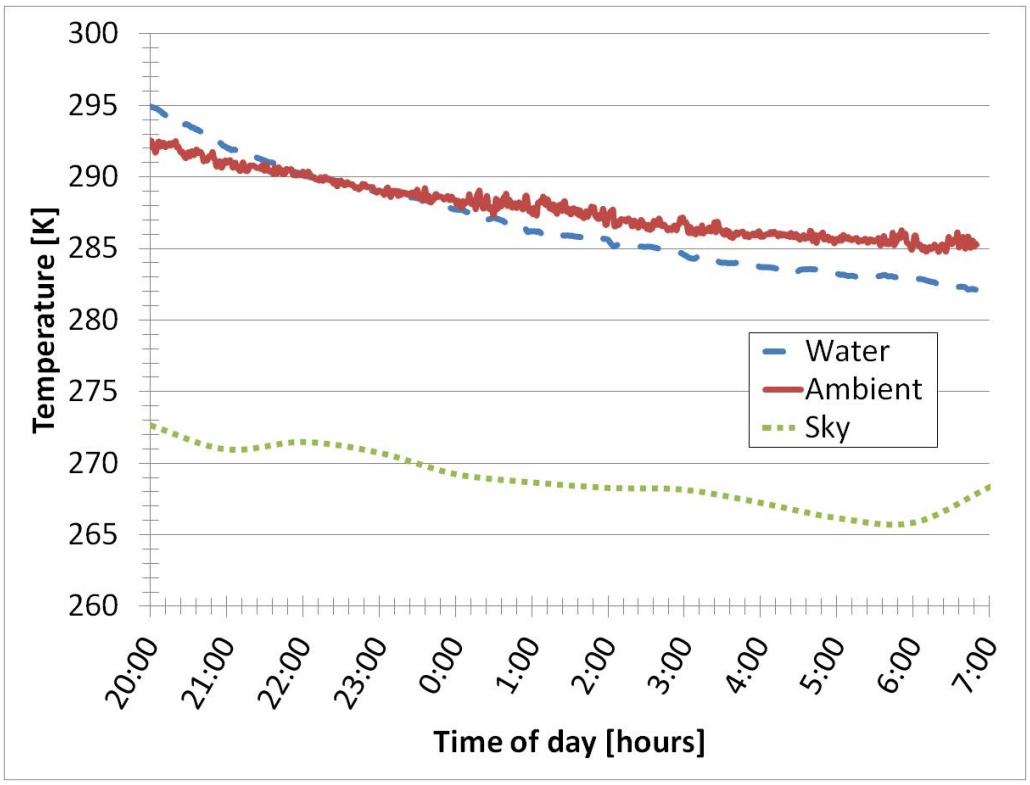

Figure 27. VIG experimental data from 10/6-7/2011 where initial ambient temp ~ water temp

The final VIG experiment had the initial condition of the water temperature being higher than the ambient temperature. This data can be seen in *Figure 28*. Again, this is data was taken from the water temperature in a 70F container. The total calculated heat flux from the data is 78.0 Wm^{-2}.

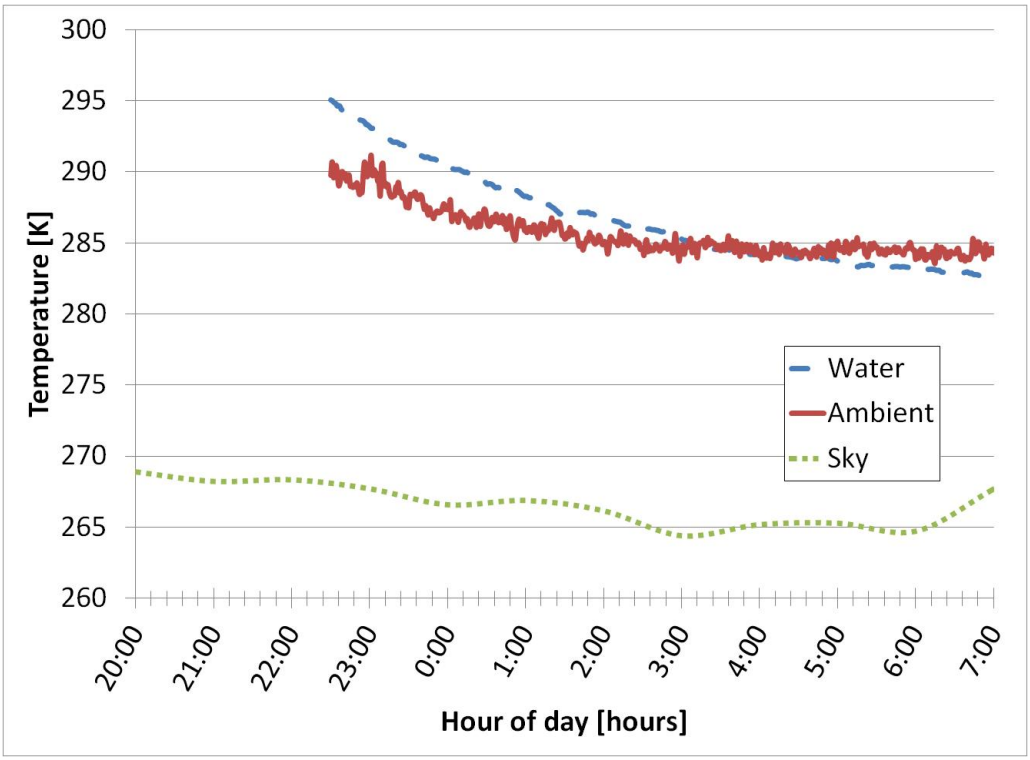

Figure 28. VIG experimental data from 10/7-8/2011 where initial ambient temp < water temp

Taking these three experiments into account, the water is certainly losing heat due to radiation and therefore scaling up the experiment up to a larger radiator size with a more practical shape is reasonable. However, the heat fluxes given all have other sources of heat loss and gain affecting them both positively and negatively depending upon the temperature of the water in relation to the ambient temperature. When the water is warmer than the ambient air, convection helps decrease the temperature and makes the system more efficient, and when the water is cooler, convection heats up the water negatively affecting the system.

Tray Radiator Results

In these experiments, the desired value is the heat flux due to radiation. As shown in the VIG experiments, calculating the heat rate over the entire night gives the entire heat flux including the effects of convection and conduction. To eliminate these modes of heat transfer, the portion of the data where the ambient temperature is the same as the water temperature should be studied. This is because the temperature difference at these points is zero, and therefore the convection and conduction heat transfer is zero. Due to the noise displayed in the ambient temperature data, a ten

minute average was used to dampen the effect. The value where the ambient temperature is the same as the water temperature was selected and then the five data points before and after were selected. These correlating heat flux points of one minute of data were averaged to determine a filtered value of the heat flux from radiation. This value was then compared with the ideal heat flux due to radiation from Equation 33.

Figure 29 shows the tray radiators being exposed to the night sky and the water temperature started out higher than the ambient temperature. Ultimately, the heat flux of the entire period is not needed. As stated previously, the best point to estimate the heat flux due to radiation is at the crossover point of the water temperature and the ambient temperature. For this set of data, that crossover point has a heat flux of 68.50 Wm^{-2} for the clear PE and 56.35 Wm^{-2} for the white PE. The radiation efficiencies at these points are 0.84 and 0.71 for the clear PE and white PE, respectively. All of this data along with other experimental data can be found in Table 4 at the end of this section.

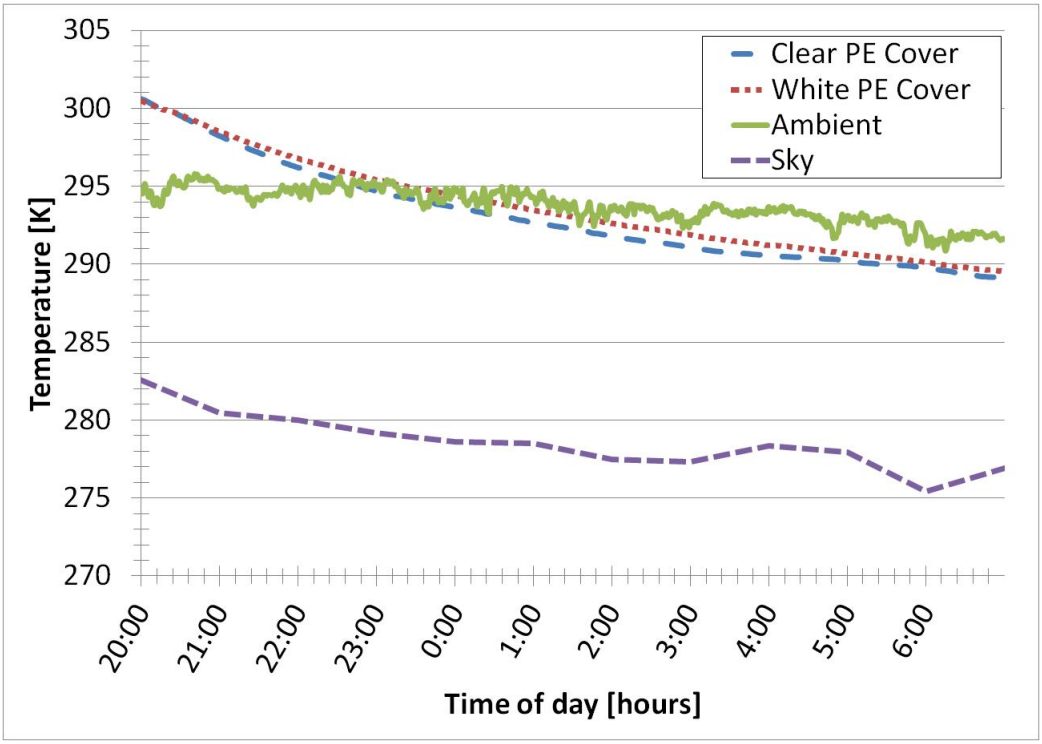

Figure 29. Tray experimental results of a clear PE cover to a white PE cover; Run on 10/25-26

The data in *Figure 30* displays an experiment run where the radiator with the clear PE cover had the view of the night sky blocked by an opaque board. This was done to show that the temperature decrease, when the temperature of the water is already below the ambient, is caused by radiation. The water with the opaque board only decreases in temperature because of

convection and conduction. The temperature of the water never drops below the ambient temperature. The heat flux at the crossover point for the white PE cover is 98.61 Wm^{-2} and the radiator efficiency is calculated to be 0.86.

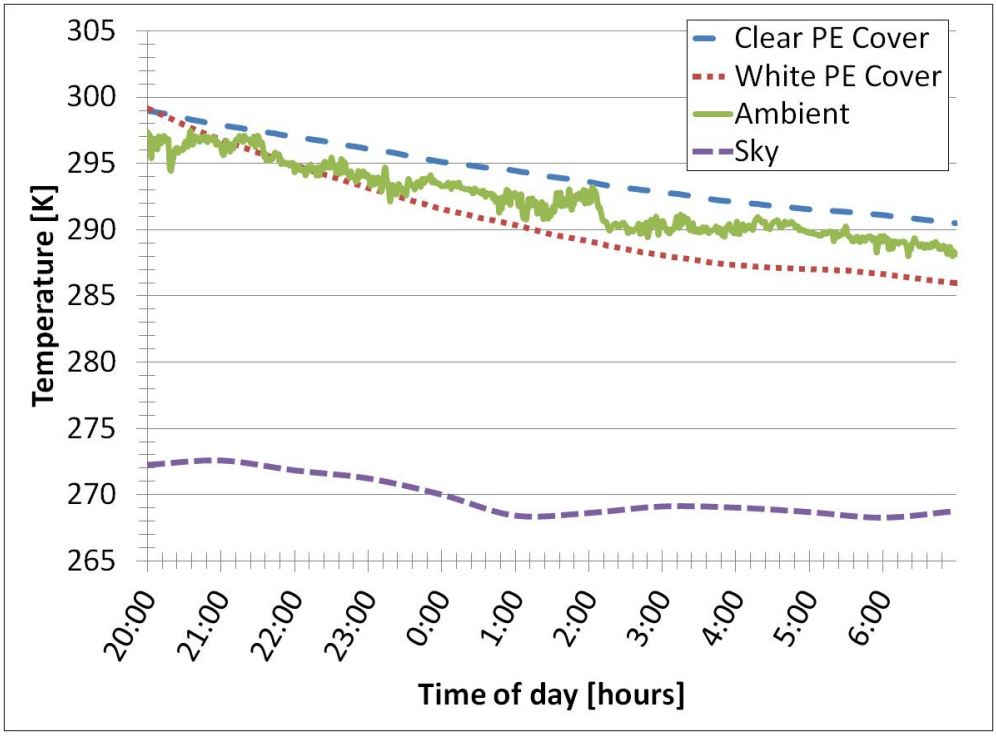

Figure 30. Tray experimental results where the clear PE is covered with an opaque board eliminating radiation; Run on 10/30-31

The last figure of the section, *Figure 31*, shows the data from the final tray experiment run comparing the white PE cover to a conventional black painted aluminum cover. The temperatures of the water for both radiators follow each other closely. The radiant heat flux at the crossover point for the clear PE cover is 37.5 Wm^{-2} while the heat flux for the aluminum cover at its crossover point is 56.35 Wm^{-2}. The radiator efficiency for the PE cover is 0.46 and for the aluminum cover is 0.67.

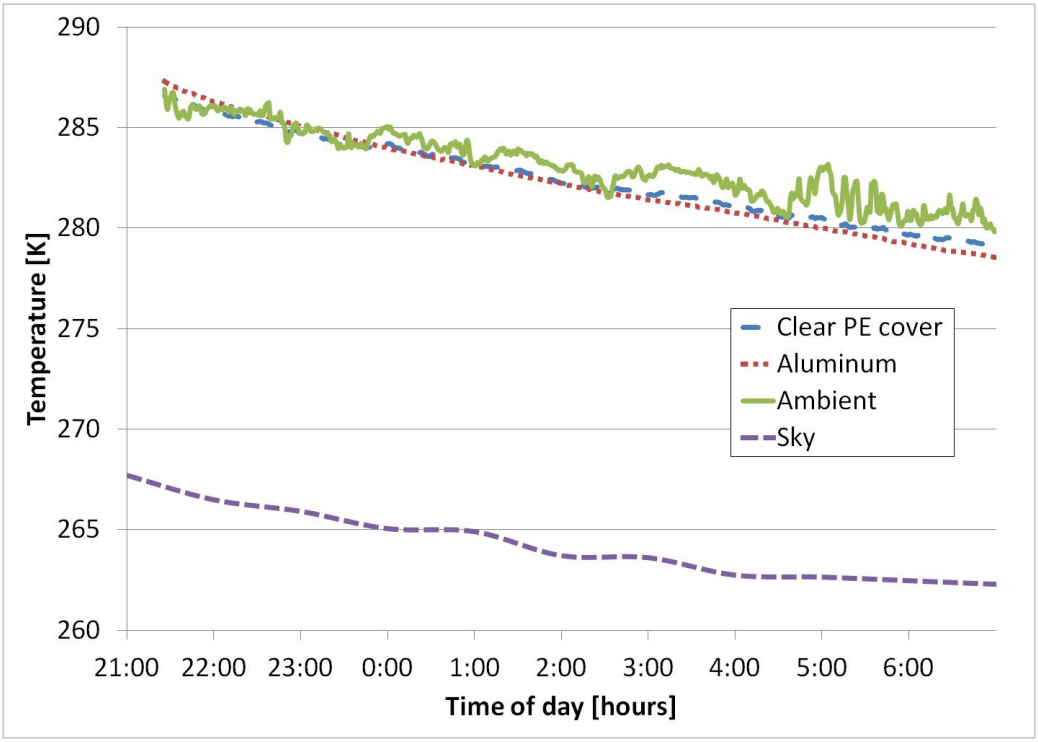

Figure 31. Tray experimental results comparing a clear PE cover to a black aluminum foil cover

Table 4. *Experiment data and calculations at ambient and water crossover point*

Date	PE Cover	Time [s]	T_{water} [K]	T_{∞} [K]	T_{sky} [K]	$q''_{rad,\,total}$ [Wm^{-2}]	$q''_{rad,\,ideal}$ [Wm^{-2}]	$\frac{q''_{rad,total}}{q''_{rad,ideal}}$
10/24-25	White	0:53	298.00	297.81	278.80	48.52	104.56	0.46
10/25-26	Clear	22:30	295.40	295.20	279.60	68.50	81.83	0.84
10/25-26	White	0:20	294.10	294.14	278.50	56.35	79.79	0.71
10/27-28	Clear	22:36	290.53	290.66	269.15	67.39	102.18	0.66
10/27-28	White	22:36	290.37	290.66	269.15	90.78	101.34	0.89
10/30-31	White	21:59	294.91	294.82	271.81	98.61	114.60	0.86
11/25-26	White	23:34	284.18	284.14	266.20	37.57	81.66	0.46
11/25-26	Alum	23:18	284.74	284.66	266.30	56.35	84.08	0.67

Experimental Uncertainty

The root sum square method was used to determine the experimental uncertainty of the data collected. The three sources of error in the measurement came from the thermocouples, the CR23X Micrologger, and the volume of the water. The thermocouples had an error of 0.2^{o}C when first calibrated. The CR23X operations manual states an error of 0.025% when recording temperature data between 0 and 20^{o}C. The error in the volume of water is due to leaks in the system. The error is +/- 1 liter of water. The assumed volume is 17 liters. The root sum squares method can be described as the following

$$\frac{u_q}{q} = \sqrt{\left(\frac{u_T}{T}\right)^2 + \left(\frac{u_V}{V}\right)^2} \tag{34}$$

where u_q/q is the percent uncertainty in the heat rate which can be directly correlated to heat flux, u_T is the uncertainty in the temperature, and u_V is the uncertainty in the volume. For this analysis, the temperatures of 10 and 20^{o}C will be considered because that is the range of temperatures in which this experiment occurs. At these selected temperatures the uncertainly from the Micrologger can be neglected because it is much smaller than the uncertainty from the thermocouples. At 20^{o}C the uncertainty percentage of q" is 5.97% while the percent uncertainty of q" at 10^{o}C is 6.21%. It can be seen that the lower the temperature goes, the higher the percent uncertainty becomes.

DISCUSSION & CONCLUSION

The vacuum insulated glass experiments showed that no matter the initial temperature of the water relative to the ambient temperature, radiation can create a heat flux that will cool the water throughout the course of the night. Even when the water temperature was below the ambient temperature, a radiant heat flux of 33.7 Wm^{-2} was achieved. When considering the negative effects of conduction and convection, this number is certainly higher. The VIG experiments that started with a higher water temperature had much higher radiant heat fluxes with values around 80 Wm^{-2}. While these cannot be directly attributed to radiation due to other heat transfer mode effects, it is clear that radiation helps decrease the temperature of the water and ultimately the experiment must be scaled up to a more appropriate size such as the tray radiators.

The data from the tray radiator experiments shows promise for the fluid emission concept. All the radiant heat fluxes at the crossover points have values higher than 35 Wm^{-2} with the highest value of 98.61 Wm^{-2} coming from the radiator with the white PE cover. The white PE cover also had the highest radiation efficiency of 0.86. The most important experimental results are from the final experiment comparing the aluminum cover to the white PE cover. The aluminum cover outperformed the clear PE cover with radiant heat flux of 56.35 Wm^{-2} compared to 37.57 Wm^{-2}. These resulted in radiator efficiencies of 0.67 and 0.46, respectively. The values in Table 4 compare well to the model value of 76.67 Wm^{-2} for the heat flux, but do not compare as well for the radiator efficiency of 0.91. Comparing these results to the ones achieved by other researchers mentioned in the Background section, these experiments were much more effective. One potential reason for the higher radiant heat flux may be due in part to geographic location and therefore climate where the experiments took place. Phoenix, AZ is very dry which means it has a lower dew point than most places. This lower dew point directly affects the sky temperature by causing it to be lower and thus creates a larger temperature difference between the water and its heat sink, the night sky. Another potential reason for the differences may be because the system is not flowing, but without studying a flowing system, this remains in question.

An issue with these experiments and analysis originates from the ambient temperatures. First, the thermocouple used was very sensitive and has quite a bit of noise during portions of the

varying experiments. Essentially, the two temperatures could cross multiple times due to the noise in the ambient temperature data. This created the need to average the one minute recorded heat fluxes over a ten minute period. Another issue is that the actual dew point temperature may be slightly different than the dew point temperature data used from the ASU Weather Station. This may have resulted in a less accurate sky temperature.

The cover materials used in the experiments all proved to be somewhat similar. The two PE covers provided very comparable results. The white PE was chosen for comparison to the aluminum cover because of the results from the FTIR analysis even though when directly compared with the clear PE, it was outperformed during one experiment as shown in Table 4. Potentially, the clear PE cover could outperform the white PE if it were as thin as the white PE. However, a system would need to be able to survive many years in the natural environment to be cost effective. Thicker polyethylene may need to be studied to determine if it can still be a good infrared transmitter when made to be more durable.

It is recommended that research in this area continue so that a more direct comparison to the studies performed by other engineers and scientists can be made. In particular, the direct fluid radiative cooling system described in this paper should be modified into a flowing system. This would give a more accurate depiction of whether or not a similar system could be ultimately utilized in a power plant cooling process.

FUTURE WORK

Based on the experimental data given in this thesis, further studying the potential for direct fluid radiative cooling would be recommended. Many things could be done to improve upon the experiments run. The first step should be to better insulate the tray radiators. While the VIG containers were well insulated, the trays were significantly affected by convection. If possible, vacuum insulated trays would be ideal. Based on the current shape, that may not be possible. A potential variation to the project may be to add another cover over top of the radiator, virtually eliminating all but free convection. This however would decrease the transmittance value, negatively affecting the radiative cooling value. The convective heat gains to the system should be measured against the radiative cooling losses to determine the wind speed at which point it would be beneficial to add another cover.

Testing for better cover materials would be another way to improve the project. The materials tested were not rigid. Endurance may become an issue with the cover material due to a lack of strength. This is partly due to the reasoning that cheap materials mean a more economical radiator. It would also be worth testing materials found in nature such as BaF_2 or AgBr, known to have high transmissivity in the appropriate IR range (Beamlines, 2011), to see if radiative cooling is improved.

Once the ideal non-flowing system is determined, the next step should be making the system flow. Many of the radiative cooling systems used for comparison in this paper were flowing systems. A direct comparison of a flowing system with a clear cover to a flowing system using a metal radiator would be useful to determine which system would be more effective to cool a fluid. An economic analysis should also be performed to determine the cost of a system with metal radiators compared to a system with IR transparent cover radiators.

Another way to improve the radiative heat transfer is to increase the area being radiated. One possible way to do this is to tilt the radiators. This would increase the area being radiated while keeping the footprint the same. A more in depth study of radiation shape factors would need to be performed for this experiment. One last idea to increase the radiation performance of the system would be to utilize phase change materials in the water. The goal would be to capture more

heat from the condenser by using materials such as waxes with a higher heat capacity than water. The waxes would be encapsulated and would transfer their heat to the water as the water is cooled during the radiation process. An alternative experiment to run that is similar to this would be using nanofluids to see if the increased surface area from the particles increases the amount of cooling from radiation.

REFERENCES

Ali, A. H., Taha, I. M., & Ismail, I. M. (1995). Cooling of water flowing through a night sky radiator. *Solar Energy* , 235-253.

American Infrared. (n.d.). *FLIR P0, FLIR P65, FLIR S60, FLIR S65 Infrared Sale Price or Rental.* Retrieved October 14, 2011, from American Infrared: http://www.americaninfrared.com/ProductDetail.asp?ID=58

Carvalho, M. d. (2010, July 7). *Radiative Heat Transfer.* Retrieved October 24, 2011, from Thermopedia (TM) BETA: http://www.thermopedia.com/content/5491/?tid=104&sn=132

Culp, A. W. (1991). *Principles of Energy Conversion.* New York: McGraw-Hill, Inc.

El-Wakil, M. M. (2002). *Powerplant Technology.* New York: The McGraw-Hill Companies, Inc.

Erell, E., & Etzion, Y. (2000). Radiative cooling of buildings with flat-plate solar collectors. *Building and Environment* , 297-305.

Incropera, F. P., Dewitt, D. P., Bergman, T. L., & Lavine, A. S. (2007). *Fundamentals of Heat and Mass Transfer 6th Edition.* Hoboken, NJ: John Wiley & Sons, Inc.

Kimball, B. A. (1985). Cooling performance and efficiency of night sky radiators. *Solar Energy* , 19-33.

Matsuta, M., Terada, S., & Ito, H. (1987). Solar heating and radiative cooling using a solar collector-sky radiator with a spectrally selective surface. *Solar Energy* , 183-186.

Michell, D., & Biggs, K. L. (1979). Radiation Cooling of Buildings at Night. *Applied Energy* , 263-275.

Moran, M. J., & Shapiro, H. N. (2004). *Fundamentals of Engineering Thermodynamics.* Hoboken, NJ: John Wiley & Sons, Inc.

Nilsson, T. M., & Niklasson, G. A. (1995). Radiative cooling during the day: simulations and experiments on pigmented polyethylene cover foils. *Solar Energy Materials and Solar Cells* , 93-118.

Perez-Garcia, M. (2004). Simplified modelling of the nocturnal clear sky atmospheric radiation for environmental applications. *Ecological Modelling* , 395-406.

Spetzler, D., & Venables, J. (2004, February 18). *Blackbody Radiation.* Retrieved October 6, 2011, from Arizona State University: http://venables.asu.edu/quant/DavidS/index.html

Universitat Politecnica de Catalunya - Barcelona Tech. (2011, March). *Infrared/UV Spectroscopy - Center for Research in NanoEngineering*. Retrieved October 26, 2011, from Universitat Politecnica de Catalunya - Barcelona Tech: http://www.upc.edu/crne/infrastructure/infrared-uv-spectroscopy

Yiping, W., Yong, C., Li, Z., & Lijun, H. (2008). Experiments on novel solar heating and cooling system. *Energy Conversion and Management* , 2083-2089.